SPRINGER BRIEFS IN APPLIED SCIENCES AND TECHNOLOGY · NANOTHERANOSTICS

Tao Feng
Yanli Zhao

Nanomaterial-Based Drug Delivery Carriers for Cancer Therapy

Springer

SpringerBriefs in Applied Sciences and Technology

Nanotheranostics

More information about this series at http://www.springer.com/series/13040

Tao Feng · Yanli Zhao

Nanomaterial-Based Drug Delivery Carriers for Cancer Therapy

Springer

Tao Feng
Division of Chemistry and Biological
Chemistry, School of Physical
and Mathematical Sciences
Nanyang Technological University
Singapore
Singapore

Yanli Zhao
Division of Chemistry and Biological
Chemistry, School of Physical
and Mathematical Sciences
Nanyang Technological University
Singapore
Singapore

ISSN 2191-530X ISSN 2191-5318 (electronic)
SpringerBriefs in Applied Sciences and Technology
ISSN 2197-6740 ISSN 2197-6759 (electronic)
Nanotheranostics
ISBN 978-981-10-3297-4 ISBN 978-981-10-3299-8 (eBook)
DOI 10.1007/978-981-10-3299-8

Library of Congress Control Number: 2016959753

Printed on acid-free paper

This Springer imprint is published by Springer Nature
The registered company is Springer Nature Singapore Pte Ltd.
The registered company address is: 152 Beach Road, #22-06/08 Gateway East, Singapore 189721, Singapore

Acknowledgements

This work is supported by the SingHealth-NTU Research Collaborative Grant (No. SHS-NTU/009/2016), and the NTU-Northwestern Institute for Nanomedicine.

Contents

About the Authors

Tao Feng received both her B.S. (in 2010) and M.S. (in 2013) degrees in Chemistry from Jilin University, China. Currently, she is pursuing her Ph.D. degree under the supervision of Prof. Yanli Zhao at Nanyang Technological University. Her research interests include developing fluorescent inorganic nanomaterials for drug delivery in cancer therapy.

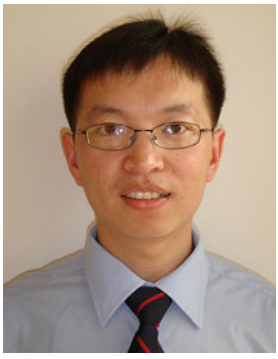

Yanli Zhao is currently Associate Professor at Nanyang Technological University, Singapore. He received his B.Sc. degree in Chemistry from Nankai University in 2000 and his Ph.D. degree in Physical Chemistry there in 2005 under the supervision of Prof. Yu Liu. He was a postdoctoral scholar with Prof. Sir Fraser Stoddart at University of California Los Angeles (October 2005–November 2008) and subsequently at Northwestern University (January 2010–August 2010). In between (December 2008–December 2009), he was a postdoctoral scholar with Prof. Jeffrey Zink at University of California Los Angeles. He has published over 250 scientific papers, and received several awards including the TR35@Singapore Award in 2012 and the Singapore National Research Foundation Fellowship in 2010. His current research focuses on the development of integrated systems for diagnostics and therapeutics, as well as porous materials for gas storage and catalysis.

Chapter 1
Current Status and Characteristics of Cancer

Cancer is among the most deadly and incapacitating disease known (Siegel et al. 2014). 13 Million new cancer cases surface annually and it is about 8 million casualties worldwide each year—13% of the total 56 million victims of all causes for death in the world. Despite numerous breakthroughs in cancer therapeutics research, 16 million new cancer cases are expected to materialize by 2020. 5 Major forms of cancer contributing to mortality globally are stomach, liver, colorectal, lung and breast cancer. Within the European Union (EU), breast cancer is diagnosed every 2.5 min and a female falls victim to this disease every 7.5 min. Lung cancer remains the most prevalent cancer worldwide and is responsible for 1.2 million new cases annually (Hesketh 2013). The prognosis of cancer is poor if advanced or late stage cancer is diagnosed or if the tumor is found to be malignant. According to the National Cancer Institute, national spending for cancer care in the United States amounted to about $125 billion in 2010 and could reach staggering $156 billion in 2020. It is thus imperative to understand cancer fully in terms of its causation and its characteristics to design better treatment options for cancer patients.

The causes of cancer are mainly classified into two categories: exogenous and endogenous. The major exogenous factors that result in cancer causation are radiation, diet, tobacco smoke, increased exposure to industrial carcinogens and environmental pollution (Hesketh 2013). According to World Health Organization (WHO), tobacco use is the most critical culprit for cancer, leading to about 20% of global cancer deaths and about 70% of global lung cancer deaths. Epidemiological studies conclude that the dominant driving forces for developing liver cancer in South-East Asians are exposure to dietary aflatoxins and infection with hepatitis viruses (Shuker 2007). The main endogenous factors that account for cancer diagnosis are polygenetic disorders, genetic mutations (missense or silent mutations, insertions and deletions), DNA mutations (chromosomal translocations and gene amplification), dysregulation in cell signaling, overexpression of surface receptors, enzymes and genes, and dysregulation of the replication, transcription and translation machinery, cell cycle (Hesketh 2013).

T. Feng and Y. Zhao, *Nanomaterial-Based Drug Delivery Carriers for Cancer Therapy*, Nanotheranostics, DOI 10.1007/978-981-10-3299-8_1

Table 1.1 Comparison of the properties of cancer tissues with normal tissues

Parameters	Normal tissues	Cancer tissues
Metabolism	Functional	Abnormal
Temperature	Body temperature	Elevated, abnormal temperature gradients
Lymphatic system	Rapid clearance, functional	Lack of lymphatic drainage
Interstitial pressure	Normal	High
Blood flow	Regular and continuous	Irregular and discontinuous
Vasculature architecture/morphology	Ordered, normal branching Low Permeability Even diameter of vessels	Chaotic, disorganized, abnormal branching High permeability, leaky, hypervasculature Uneven diameter of vessels
Pore size/nm	2–60	100–780
pH of microenvironment	Physiological (7.4)	Mildly acidic (6.8)
Inflammation	Absence	Presence
Partial pressure of oxygen	Normal	Low (hypoxia)
Enzymes (MMP, telomerase, ALP) expression	Normal	High
Redox environment	Normal	Reductive in cytosol, oxidative in mitochondria
Expression of markers	Consistent, balanced	Imbalance of pro- and anti-angiogenic cues

Thanks to advances in high-throughput genotyping and proteomics tools to identify potential tumor biomarkers, early cancer detection is possible (Michener et al. 2002; Koomen et al. 2008). Several tumor biomarkers have been identified for early cancer diagnosis: hypermethylation of p16, KRAS, BRAF and p53 mutations, to name a few (Coppedè et al. 2014; Ng and Yu 2015). Compared with normal tissues, cancerous tissues possess considerable physiological and morphological differences in temperature, metabolism machinery, oxygen content, pH, and expression of enzymes and markers, which are briefly summarized in Table 1.1.

1.1 Abnormal Metabolism

Metabolic perturbations are biochemical signatures of cancer cells (Ganapathy-Kanniappan and Geschwind 2013). Most of its energy is obtained from glucose in glycolysis, rather than from pyruvate's oxidative breakdown in the mitochondria. Even in the presence of abundant oxygen, glucose is converted to lactate, which usually occurs anaerobically (Gatenby and Gillies 2004). The aerobic glycolysis is also known as the Warburg effect (Vander Heiden et al. 2009). As the

tumor cells have a need to generate glucose, the glycosidase enzyme α-amylase that catalyzes the conversion of starch to glucose was reported to be 85-fold more concentrated in the tumor microenvironment (TME) (De la Rica et al. 2012). Due to the active metabolism of tumor cells, lactic acid accumulation and insufficient blood supply, the TME is highly acidic (Stubbs et al. 2000). To satisfy metabolic needs, hypoxic tumors trigger the angiogenic switch to form new vessels (Bergers and Benjamin 2003).

1.2 Abnormal Vasculature

In normal tissues, vessels are organized in a hierarchical manner such that all cells are proximal to their vessels, and nutrients can be easily diffused and completely consumed until they reach their targets (Siemann 2011). Compared to normal vasculature, tumor vasculature architecture is often disorganized and heterogeneous, and lacks the ordered branching network of normal vessels (Narang and Varia 2011). In tumors, vessel organization is aberrant and non-canonical, and vessel diameters are non-uniform (Dudley 2012). Besides, tumor vessels have poor pericyte cover (responsible for vasoconstriction), and arterioles and venules are difficult to distinguish from each other, which contribute to the high degree of disorder (Matsumura and Maeda 1986; Dvorak 2003). Blood flow through the tumor capillaries is sluggish and sometimes stationary (Munn 2003). Hence, the high irregularity, intermittent and discontinuous nature of the blood flow leads to the entire TME, including the red blood cells and endothelium to be highly hypoxic. The high hypoxia enables tumors to develop new blood vessels (extensive angiogenesis), and as a result, high vascular density of tumors is common (Maeda et al. 2000).

The copious amounts of vascular permeability factors and mediators such as nitric oxide (NO), carbon monoxide (CO), bradykinins, vascular endothelial growth factor (VEGF), kallikrein proteases and peroxynitrite present all account for the leaky microvasculature and hyperpermeability due to the large gaps and pores that reside between endothelial cells (Fang et al. 2011).

1.3 Resistance to Anti-proliferative Growth Factors (GFs)

Elevated levels of pro-angiogenic VEGF persist in cancer cells, and angiogenic regulators such as anti-angiogenic angiostatin and endostatin are often in dearth (Carmeliet and Jain 2000). Transforming growth factor (TGF)-β, whose function is ablated in tumor cells, accounts for anaplasia or loss of differentiation in tumor cells (Wakefield et al. 2000).

1.4 Unlimited Replicative Potential

Telomerase, an enzyme preventing the degradation of telomeres and causing the cells to be immortalized, is overexpressed in cancer cells (Gupta and Qin 2003; Hanahan and Weinberg 2011). They can also engage in alternative telomere lengthening (ALT)—a process of recombination between telomeres of various chromosomes. These autonomous cancer cells are independent of growth signals and other molecular cues that prompt them to proliferate.

1.5 Immune System Activation and Inflammation

Pro-inflammatory cytokines are often secreted in tumor cells (Dinarello 2000). Tumor-associated macrophages (TAMs) constitute the bulk of the immune cells found in the TME. The cytokines TAM release could activate the expression of VEGF, cyclooxygenases (COX2), epidermal growth factor receptor (EGFR), matrix metalloproteinases (MMPs) (Goldberg and Schwertfeger 2010; Koontongkaew 2013).

1.6 Interstitial Pressure

The tumor interstitial fluid pressure (TIFP) in solid tumors is particularly elevated (14–30 mmHg for cancers) as compared to normal tissues (0 mmHg) due to the richly developed and highly permeable vascular networks, as well as the presence of non-functional lymphatic circulation (Torchilin 2011; Spencer et al. 2015). This fact also forms a barrier against the uptake of chemotherapeutics and a lack of treatment efficacy.

References

Bergers G, Benjamin LE (2003) Angiogenesis: tumourigenesis and the angiogenic switch. Nat Rev Cancer 3:401–410

Carmeliet P, Jain RK (2000) Angiogenesis in cancer and other diseases. Nature 407:249–257

Coppedè F, Lopomo A, Spisni R, Migliore L (2014) Genetic and epigenetic biomarkers for diagnosis, prognosis and treatment of colorectal cancer. World J Gastroenterol 20:943–956

De la Rica R, Aili D, Stevens MM (2012) Enzyme-responsive nanoparticles for drug release and diagnostics. Adv Drug Deliv Rev 64:967–978

Dinarello CA (2000) Proinflammatory cytokines. Chest 118:503–508

Dudley AC (2012) Tumor endothelial cells. Cold Spring Harb Perspect Med 2:a006536

Dvorak HF (2003) How tumors make bad blood vessels and stroma. Am J Pathol 162:1747–1757

Fang J, Nakamura H, Maeda H (2011) The EPR effect: unique features of tumor blood vessels for drug delivery, factors involved, and limitations and augmentation of the effect. Adv Drug Deliver Rev 63:136–151

Ganapathy-Kanniappan S, Geschwind JFH (2013) Tumor glycolysis as a target for cancer therapy: progress and prospects. Mol Cancer 12:152

Gatenby RA, Gillies RJ (2004) Why do cancers have high aerobic glycolysis. Nat Rev Cancer 4:891–899

Goldberg JE, Schwertfeger KL (2010) Proinflammatory cytokines in breast cancer: mechanisms of action and potential targets for therapeutics. Curr Drug Targets 11:1133–1146

Gupta MK, Qin RY (2003) Mechanism and its regulation of tumor-induced angiogenesis. World J Gastroenterol 9:1144–1155

Hanahan D, Weinberg RA (2011) Hallmarks of cancer: the next generation. Cell 144:646–679

Hesketh R (2013) Introduction in cancer biology: a concise journey from epidemiology through cell and molecular biology to treatment and prospects. Cambridge University Press, New York

Koomen JM, Haura EB, Bepler G, Sutphen R, Remily-Wood ER, Benson K, Dalton WS (2008) Proteomic contributions to personalized cancer care. Mol Cell Proteomics 7:1780–1794

Koontongkaew S (2013) The tumor microenvironment contribution to development, growth, invasion and metastasis of head and neck squamous cell carcinomas. J Cancer 4:66–83

Maeda H, Wua J, Sawaa T, Matsumurab Y, Horic K (2000) Tumor vascular permeability and the EPR effect in macromolecular therapeutics: a review. J Control Release 65:271–284

Matsumura Y, Maeda H (1986) A new concept for macromolecular therapeutics in cancer chemotherapy: mechanism of tumoritropic accumulation of proteins and the antitumor agent smancs. Cancer Res 46:6387–6392

Michener CM, Ardekani AM, Petricoin EF, Liotta LA, Kohn EC (2002) Genomics and proteomics: application of novel technology to early detection and prevention of cancer. Cancer Detect Prev 26:249–255

Munn LL (2003) Aberrant vascular architecture in tumours and its importance in drug-based therapies. Drug Discov Today 8:396–403

Narang AS, Varia S (2011) Role of tumor vascular architecture in drug delivery. Adv Drug Deliv Rev 63:640–658

Ng JMK, Yu J (2015) Promoter hypermethylation of tumour suppressor genes as potential biomarkers in colorectal cancer. Int J Mol Sci 16:2472–2496

Shuker DEG (2007) Socioeconomic and molecular basis of cancer. In: Missailidis S (ed) The cancer clock. Wiley, Chichester, pp 3–24

Siegel R, Ma J, Zou Z, Jemal A (2014) Cancer statistics. CA Cancer J Clin 64:9–29

Siemann DW (2011) The unique characteristics of tumor vasculature and preclinical evidence for its selective disruption by tumor-vascular disrupting agents. Cancer Treat Rev 37:63–74

Spencer DS, Puranik AS, Peppas NA (2015) Intelligent nanoparticles for advanced drug delivery in cancer treatment. Curr Opin Chem Eng 7:84–92

Stubbs JM, McSheehy PM, Griffiths JR, Bashford CL (2000) Causes and consequences of tumour acidity and implications for treatment. Mol Med Today 6:15–19

Torchilin V (2011) Tumor delivery of macromolecular drugs based on the EPR effect. Adv Drug Deliv Rev 63:131–135

Vander Heiden MG, Cantley LC, Thompson CB (2009) Understanding the Warburg effect: the metabolic requirements of cell proliferation. Science 324:1029–1033

Wakefield LM, Yang Y, Dukhanina O (2000) Transforming growth factor-β and breast cancer: lessons learned from genetically altered mouse models. Breast Cancer Res 2:100–106

Chapter 2
Clinical Anticancer Drugs for Cancer Treatment

Besides cytoreductive surgery and radiotherapy, chemotherapy is the most widely used therapeutic strategy in combating cancer. The high incidence of cancer has led to a lot of immunotherapeutic and chemotherapeutic drugs to be developed and approved by U.S. Food and Drug Administration (FDA). Antineoplastic agents (approved or under development) can be broadly classified into:

(1) Antimetabolites: methotrexate, fluoropyrimidines (e.g. 5-fluorodeoxyuridine (5-FU), and capecitabine), cytarabine, gemcitabine;
(2) Antimitotic agents: taxanes (e.g., docetaxel), vinca alkaloid (e.g. vincristine);
(3) Alkylating agents: carboplatin, cisplatin, oxaliplatin;
(4) Antitumor antibiotics: anthracyclines (e.g. doxil, daunorubicin), podophyllotoxins (e.g. etoposide, teniposide), campothecins (e.g. topotecan, irinotecan);
(5) Tyrosine kinase inhibitors (TKI): imatinib, gefinitib, dasatinib, sunitinib, afatinib, lapatinib, vismodegib;
(6) Cyclin dependent kinase (CDK) inhibitors: alvocidib, palbociclib;
(7) Poly(ADP-ribose) polymerase (PARP) inhibitors: olaparib, rucaparib, veliparib;
(8) Histone deacetylase (HDAC) inhibitors: mocetinostat, belinostat, romidepsin, vorinostat, trichostatin;
(9) Mitogen-activated protein kinase (MAPK) kinase (MEK) inhibitors: selumetinib, trametinib, cobimetinib;
(10) Serine/threonine-protein kinase B-Raf inhibitors: vemurafenib, sorafenib, dabrafenib;
(11) Mammalian target of rapamycin (mTOR) inhibitors: temsirolimus, everolimus;
(12) Phosphoinositide 3-kinase (PI3K) inhibitors: idelalisib;
(13) Ribonucleotide reductase (RNR) inhibitors: cladribine, tezacitabine, fludarabine;
(14) DNA methyltransferase inhibitors: 5-azacytidine (5-AzaC), 5′-deoxy-azacytidine (DAC);

T. Feng and Y. Zhao, *Nanomaterial-Based Drug Delivery Carriers for Cancer Therapy*, Nanotheranostics, DOI 10.1007/978-981-10-3299-8_2

(15) Retinoids: tretinoin, bexarotene;
(16) Monoclonal antibodies (mAbs): ofatumumab, ibritumomab tiuxetan, rituximab.

These antineoplastic drugs often exert their anticancer effects via several mechanisms of actions and their use in cancer treatment is briefly described below.

2.1 Antimetabolites

Methotrexate, a competitive antagonist of dihydrofolate reductase that participates in the tetrahydrofolate synthesis needed subsequently in thymidine and DNA synthesis, is employed for treating osteosarcomas and trophoblastic neoplasms. 5-FU (Adrucil), an irreversible inhibitor of thymidylate synthase, is indicated for oesophageal, stomach, pancreatic and skin cancers.

2.2 Antimitotic Agents

There are two major classes of antimitotic agents: taxanes and vinca alkaloids, which act as antithesis to each other. Taxanes inhibit tubulin depolymerization in the spindle fiber apparatus, while vinca alkaloids hamper tubulin polymerization.

Docetaxel (Taxotere), a mitotic spindle assembly inhibitor, is FDA-approved for treating locally advanced or metastatic breast cancer, non-small cell lung cancer (NSCLC), head and neck cancer, gastric cancer and hormone-resistant prostate cancer. Vincristine (Oncovin), an inhibitor of mitotic spindle disassembly during metaphase, is widely used to treat acute myeloid leukemia (AML), acute lymphoblastic leukemia (ALL) and neuroblastoma. Vinblastine (Velban), besides preventing the microtubules formation, also hampers glutamic acid metabolism and is approved for several hematological and solid tumors. Vinorelbine (Navelbine), similar in action as vinblastine, is used for treating relapsed metastatic breast cancer.

2.3 Alkylating Agents

Carboplatin (Parapatin), oxaliplatin (Eloxatin) and cisplatin, which crosslink guanine residues, are effective in several forms of cancer. They are able to form inter-strand and intra-strand crosslinks on the guanine residues via the coordination of the N_7 atoms of the purine bases to platinum. The crosslinking ultimately stalls the action of DNA and RNA polymerases. Chlorambucil (Leukeran), a DNA replication interferent, acts against chronic lymphoid leukemia (CLL). All of these agents belong to the WHO's List of Essential Medicines.

2.4 Antitumor Antibiotics

Mitomycin C is FDA-approved for the treatment of adenocarcinomas of the stomach and pancreas, while bleomycin is employed in squamous cell cancer, Hodgkin's disease and germ cell tumors. Doxorubicin (DOX, Adriamycin), a planar anthracycline glycoside antibiotic which intercalates between DNA bases and DNA topoisomerases inhibitor, is a first-line drug for many cancer types, but is primarily used in breast carcinoma, pediatric solid tumors, ovarian cancer and Hodgkin's disease. Etoposide (Etopophos) and teniposide (Vumon) are both DNA topoisomerase II inhibitors for the utilization in leukemia treatment. Irintoecan (Camptosar) and topotecan (Hycamtin) belong to the campothecin family. Both of these DNA topoisomerase I inhibitors are FDA-approved for the treatment of refractory metastatic colon cancer and relapsed ovarian carcinoma, respectively.

2.5 Tyrosine Kinase Inhibitors (TKI)

Gefitinib (Iressa), Afatinib (Gilotrif) and Erlotinib (Tarceva) are widely used to treat NSCLC. Imatinib (Gleevec), another popular TKI that binds to the kinase domain of abelson murine leukemia viral oncogene homolog 1 (abl) in the bcl-abl fusion protein, was approved by FDA in 2001 for treating chronic myeloid leukemia (CML). In 2006, TKI Sunitinib (Sutent) was the first anticancer drug simultaneously approved for two different indications: renal cell carcinoma (RCC) and imatinib-resistant gastrointestinal stromal tumor (GIST). Vandetanib (Caprelsa) inhibits a rearrangement during transfection (RET)-tyrosine kinase as well as vascular endothelial growth factor receptor (VEGFR), and was FDA-approved for the treatment of late-stage (metastatic) medullary thyroid cancer. Lapatinib (Tykerb), a less commonly known TKI, interrupts the human epidermal growth factor receptor 2 (HER2/neu) and EGFR pathways, and is utilized to treat breast cancer.

2.6 Cyclin Dependent Kinase (CDK) Inhibitors

Alvocidib (Flavopiridol), a flavonoid alkaloid CDK9 kinase inhibitor, interferes with RNA polymerase transcription and halts the cell cycle, which is under clinical development for AML treatment. Palbociclib (Ibrance), a CDK4 and CDK6 inhibitor, is used for treating estrogen receptor (ER)-positive and HER2-negative breast cancer.

2.7 Poly(ADP-Ribose) Polymerase (PARP) Inhibitors

Olaparib (Lynparza) is an FDA-approved targeted therapeutic agents for cancer. Rucaparib and Veliparib are under investigation for use as anticancer agents.

2.8 Histone Deacetyltransferase Inhibitors (HDACi)

Romidepsin (Istodax) was approved in the US for the use against peripheral and cutaneous T-cell lymphoma (PTCL and CTCL). Vorinostat (Zolinza) is FDA-approved for the treatment of CTCL. Mocetinostat, another HDACi, is undergoing clinical trials for treating follicular lymphoma, Hodgkin's lymphoma and AML.

2.9 Mitogen-Activated Protein Kinase (MAPK) Kinase (MEK) Inhibitors

MEK inhibitors hamper the action of the MAPK enzyme (MEK) in the MAPK/extracellular signal-regulated kinase (ERK) pathway. Recently, Cobimetinib (Cotellic), a MEK inhibitor, is FDA-approved to treat advanced melanoma in patients who possess serine/threonine-protein kinase B-Raf proto-oncogene (BRAF) mutations in conjunction with vemurafenib (Zelboraf). Trametinib (Mekinist), a MEK1 and MEK2 inhibitor, was approved in 2013 for metastatic melanoma, while Binimetinib is in phase III clinical trial for neuroblastoma RAS viral oncogene homolog (NRAS)-mutant melanoma.

2.10 Serine/Threonine-Protein Kinase B-Raf Inhibitors

Sorafenib (Nexavar), a FDA-approved drug in 2005 to treat RCC and hepatocellular carcinoma, functions by inhibiting proto-oncogene serine/threonine-protein kinase, platelet-derived growth factor (PDGF) and VEGF. Vemurafenib (Zelboraf) is used for late-stage melanoma.

2.11 Mammalian Target of Rapamycin (MTOR) Inhibitors

Everolimus (Afinitor), an mTOR inhibitor, is FDA-approved for advanced kidney cancer, subependymal giant cell astrocytoma (SEGA), progressive neuroendocrine tumors of pancreatic origin (PNET) and HER2-negative breast cancer in

conjunction with exemestane. Another mTOR inhibitor, Temsirolimus (Torisel), was approved for treating advanced RCC.

2.12 Phosphoinositide 3-Kinase (PI3K) Inhibitors

PI3K inhibitors hinder the PI3K enzymes, which play a significant role in PI3K/protein kinase B (AKT)/mTOR pathway. The first FDA-approved anticancer PI3K inhibitor is Idelalisib (Zydelig) in 2014 to treat various leukemia types. Several other PI3K inhibitors such as Buparlisib and Duvelisib are in Phase III trials.

2.13 Ribonucleotide Reductase (RNR) Inhibitors

RNR inhibitors block the RNR enzyme action by catalyzing deoxyribonucleotides from ribonucleotides. Cladribine and fludarabine (Fludara) are employed for hematological malignancies and hairy cell leukemia (HCL), respectively, while gemcitabine (Gemzar) is used in various carcinomas, NSCLC, pancreatic, bladder, and breast cancer.

2.14 DNA Methyltransferase Inhibitors

Agents such as 5-azacytidine (5-AzaC) and 5′-deoxy-azacytidine (DAC) inhibit the action of DNA methyltransferase that is responsible for DNA methylation.

2.15 Retinoids

There are two different types of retinoid receptors that counteract each other: retinoid X receptor (RXR) and retinoic acid receptor (RAR) that are responsible for the induction of apoptosis and proliferation, respectively. Bexarotene (Targretin) is an FDA-approved RAR activator for CTCL.

2.16 Monoclonal Antibodies (MAbs)

Rituximab (Rituxan), a B cell annihilator, treats mainly lymphoma and leukemia. Trastuzumab (Herceptin), a HER2/neu receptor target, is the first mAb to receive FDA approval and used for breast cancer treatments. Ofatumumab (Arzerra) is

FDA-approved for treating CML that is fludarabine and alemtuzumab (Campath)-resistant. Tositumomab (Bexxar), an immunoglobulin (Ig) G2a anti-CD20 antibody covalently bound to ^{131}I, is also FDA-approved for rituximab-resistant lymphomas expressing CD20. Gemtuzumab ozaogamicin (Mylotarg), an anti-CD33 mAb linked to calicheamicin cytotoxic agent, is FDA-approved for AML in 2000. Panitumumab (Vectibix) targets the extracellular ligand-binding domain of EGFR and is used for patients with non-curable colorectal cancer.

2.17 Combination Therapy

Multidrug resistance (MDR) that results in refractory diseases often necessitates the use of a set of chemotherapy drugs to exert more potent cytotoxic activity against tumor cells (Gottesman 2002; Szakacs et al. 2006). Several factors account for the emergence of MDR, which include increased drug efflux due to the overexpression of both ATP-binding cassette (ABC) transporters and P-glycoprotein (P-GP) (Spencer et al. 2015), alterations in cell cycle checkpoints, overactive EGFR, tyrosine kinase receptor (RTK) and AKT (Gao et al. 2014), expression of multidrug resistance-associated protein (MRP) (Szakacs et al. 2008), and presence of cancer stem cells (Dean et al. 2005). Chemotherapy drugs often act synergistically to render more cytotoxic effect against cancer cells (Mignani et al. 2015). Multidrug regimens are ubiquitously prescribed in clinical practice to combat MDR, and they work via divergent mechanisms. Well-established combination therapies include MOPPEBVCAD (mechlorethamine, vincristine, procarbazine, prednisone, epidoxirubicin, bleomycin, vinblastine, lomustine, DOX, and vindesine) for advanced Hodgkin lymphoma, EMA-CO (etoposide, methotrexate, actinomycin-D, cyclophosphamide and vincristine) for gestational trophoblastic disease (GTD), ADE (cytosine arabinoside, daunorubicin and etoposide) for AML treatment, and G-FLIP (gemcitabine, 5-FU, leucovorin, cisplatin) for pancreatic cancer.

References

Dean M, Fojo T, Bates S (2005) Tumour stem cells and drug resistance. Nat Rev Cancer 5:275–284

Gao Y, Xie J, Chen H, Gu S, Zhao R, Shao J, Lee J (2014) Nanotechnology-based intelligent drug design for cancer metastasis treatment. Biotechnol Adv 32:761–777

Gottesman MM (2002) Mechanisms of cancer drug resistance. Annu Rev Med 53:615–627

Mignani SM, Bryszewska M, Klajnert-Maculewicz B, Zablocka M, Majoral JP (2015) Advances in combination therapies based on nanoparticles for efficacious cancer treatment: an analytic report. Biomacromolecules 16:1–27

Spencer DS, Puranik AS, Peppas NA (2015) Intelligent nanoparticles for advanced drug delivery in cancer treatment. Curr Opin Chem Eng 7:84–92

Szakacs G, Paterson JK, Ludwig JA, Booth-Genthe C, Gottesman MM (2006) Targeting multidrug resistance in cancer. Nat Rev Drug Discovery 5:219–234

Szakacs G, Jakab K, Antal F, Sarkadi B (2008) Diagnostics of multidrug resistance in cancer. Pathol Oncol Res 4:251–257

Chapter 3
Nanomaterial-Based Drug Delivery Carriers for Cancer Therapy

3.1 Introduction

Standard chemotherapeutics usually suffer from several limitations, such as their toxicity, drug resistance, and low stability. In order to circumvent above limitations, nanomaterials have been used as promising candidates to deliver conventional therapeutics for cancer therapy in recent years. Nanomaterial-based drug delivery carriers have numerous advantages including increased solubility, prolonged circulation time, and improved biodistribution, by the utilization of the enhanced permeability and retention (EPR) effect or active targeting effect to alter the uptake mechanism. Herein, we summarized different types of nanomaterial-based drug delivery carriers for cancer treatment including organic, inorganic, and organic–inorganic hybrid nanomaterials. It is believed that precisely designed nanomaterials will be the next-generation therapeutic agents for cancer theranostics.

3.2 Organic Nanomaterials

In this section, some representative organic nanomaterials, including FDA-approved liposomes, polymer-based nanoparticles, supramolecular nanosystems, and other organic nanoparticles are discussed for their applications as drug nanocarriers in cancer therapy.

3.2.1 FDA-Approved Liposomes

Currently, there are three liposome nanoparticles, i.e., Doxil, DaunoXome, and Marqibo, which were approved by FDA for cancer treatment (Table 3.1,

T. Feng and Y. Zhao, *Nanomaterial-Based Drug Delivery Carriers for Cancer Therapy*, Nanotheranostics, DOI 10.1007/978-981-10-3299-8_3

Table 3.1 FDA-approved liposomes for cancer therapy. Reproduced with permission from reference (Dawidczyk et al. 2014)

Platform	Drug	d (nm)	Drug/carrier ratio	Key design feature(s)	Problem addressed
Doxil	Doxorubicin	100	10,000–15,000	Lipid encapsulation for high drug/carrier ratio, polyethylene glycol coating to evade MPS, crystallization of drug in liposome minimizes escape during circulation	Drug toxicity and adverse cardiac side effects
DaunoXome	Daunorubicin	50	~10,000	No polyethylene glycol coating, targeted by MPS resulting in slow release into circulation	Drug toxicity and adverse cardiac side effects
Marqibo	Vincristine	100	~10,000	No polyethylene glycol coating, targeted by MPS resulting in slow release into circulation	Drug toxicity and adverse cardiac side effects

Dawidczyk et al. 2014). Doxil is a PEGylated liposome with diameter about 100 nm encapsulating 10,000 DOX molecules (Barenholz 2012), which could decrease side effects like cardiotoxicity originated from DOX with high concentration. Most of the DOX in Doxil is in its solid phase and the drug concentration is beyond its solubility limit. The introduction of cholesterol in the bilayer of liposome increases the cohesiveness of bilayer and reduces the leakage of DOX, resulting in more than 98% of the circulating drug inside liposomes (Gabizon et al. 2003). Moreover, PEG coating can lead to a long circulation half time and enhanced tumor accumulation through the EPR effect (Vllasaliu et al. 2014). Unlike Doxil, DaunoXome, and Marqibo have no PEGylated lipids in the liposomes (Silverman and Deitcher 2013). DaunoXome has a diameter of 50 nm with incorporated drug of daunorubicin (Lowis et al. 2006), and Marqibo has a diameter of 100 nm with incorporated drug of vincristine (Bedikian et al. 2011). The design mechanism for these two liposomes is to enhance the uptake by mononuclear phagocyte system (MPS), and the liposome provides a reservoir from which the free drug can be released slowly into the circulation. The design strategies for the FDA-approved liposome nanoparticles could provide an important inspiration for developing more efficient therapeutic agents for cancer treatment in clinic.

3.2.2 Polymer-Based Nanoparticles

As one kind of potential drug nanocarriers for cancer therapy, polymeric nanoparticles usually possess a stealth surface made from water-soluble polymers (e.g., poly(ethylene oxide) (PEO), poly(ethylene glycol) (PEG), poly(acrylic acid) (PAA), and dextran) and biodegradable aliphatic polymers (e.g., poly(lactide-co-glycolide) (PLGA), polylactide (PLA), and poly(ε-caprolactone) (PCL)) with size of 20–250 nm (Aw et al. 2013). The preclinical or clinical researches have confirmed that drug-loaded polymeric nanoparticles have better drug bioavailability, extended circulation time, improved accumulation in the tumor sites through the EPR effect, and reduced side effects toward normal tissues. However, polymeric nanoparticles often have inadequate stability and slow biodegradation, leading to the drug leakage during circulation and slow drug release upon the arrival at the pathological sites (Cheng et al. 2013). In recent years, various stimulus–responsive (such as pH, redox, temperature, glucose, enzymes or ultrasound, light, and magnetic field) polymeric nanoparticles have been fabricated to solve the above problems for efficient cancer treatment (Ge and Liu 2013).

Bae et al. (2007) conjugated DOX onto the polymer chains of a diblock copolymer PEG-*b*-poly(aspartic acid) through a pH-responsive hydrazone bond (PEG-*b*-P(Asp-Hyd-ADR)). The polymeric micelles assembled from PEG-*b*-P(Asp-Hyd-ADR) could release DOX under acidic environment of endosomes or lysosomes to exhibit efficient anticancer activity with low toxicity. Moreover, by introducing targeting ligand folic acid on the surface of polymer micelles, higher therapeutic efficiency and lower side effects in vivo could be achieved for tumor-bearing mice. Dai et al. (2011) fabricated redox and pH dual-responsive interfacially crosslinked micelles from a triblock copolymer PEG-*b*-poly(L-aspartic acid/mercaptoethylamine)-*b*-poly(L-aspartic acid/2-(diisopropylamino) ethylamine) (mPEG-PAsp(MEA)-PAsp(DIP)) through self-assembling at pH 10 and subsequent oxidative crosslinking to improve micelle stability in extracellular environment (Fig. 3.1). The crosslinked micelles showed good stability without the drug leakage at neutral pH, and DOX could be released at pH 5.0 or in the presence of 1,4-dithiothreitol (DTT), with the fastest DOX release under the condition of pH 5.0 and 10 mM DTT. In vivo studies exhibited that the prepared micelles had decreased drug leakage during blood circulation and improved therapeutic effects towards nude mice with Bel-7402 xenograft, when compared with DOX-loaded PEG-PCL micelles or free DOX. Qiao et al. (2011) prepared temperature, pH, and redox multi-sensitive nanogels through the copolymerization of 2-(5,5-dimethyl-1,3-dioxan-2-yloxy) ethyl acrylate (DMDEA), monomethyl oligo(ethylene glycol) acrylate (OEGA), and bis(2-acryloyloxyethyl) disulfide (BADS) (Fig. 3.2). The nanogels shrank to 17–35 nm to load drugs when the temperature increased to 37 °C, and they could swell to release drugs at acidic condition (pH 4–6) and 20 mM DTT at pH 7.4 due to the hydrolysis of the ortho ester groups or cleavage of disulfide

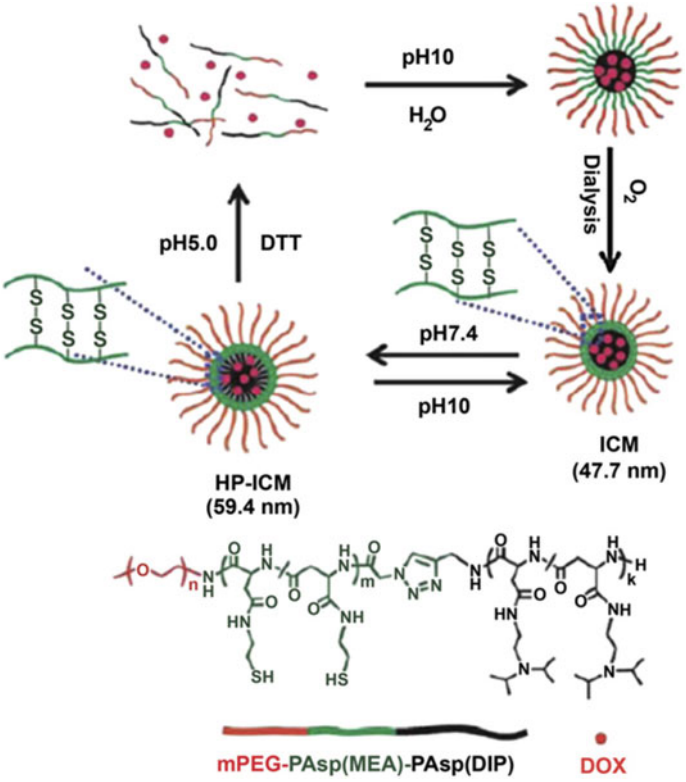

Fig. 3.1 Schematic illustration of redox and pH dual-responsive interfacially crosslinked micelles prepared from mPEG-PAsp(MEA)-PAsp(DIP). Reproduced with permission from reference (Dai et al. 2011)

crosslinkers. The nanogels without drug loading exhibited little toxicity, while the nanogels with paclitaxel (PTX) loading showed a concentration-dependent toxicity to MCF-7 cells. The results demonstrated that the multi-responsive nanogels had a great potential for the delivery of hydrophobic anticancer drugs.

3.2.3 Supramolecular Nanosystems

Since Lehn, Cram, and Pedersen won the Nobel Prize in 1987 for their discovery in supramolecular chemistry, supramolecular nanosystems based on macrocyclic hosts (such as crown ethers, cyclodextrins (CDs), cucurbit[n]urils (CBs), calixarenes (CAs), and pillar[n]arenes, Fig. 3.3) and guest molecules have received worldwide attention in recent years (Lehn 1988; Ma and Zhao 2015). The guest molecules are usually encapsulated in the cavities of macrocyclic hosts through specific molecular

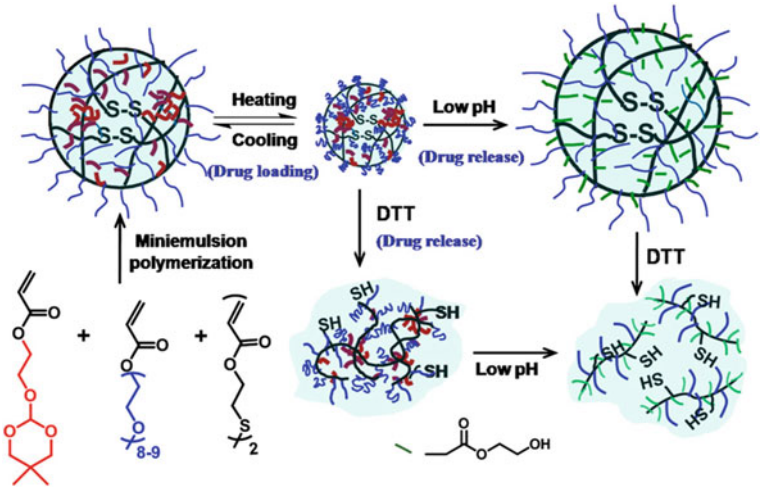

Fig. 3.2 Schematic illustration of temperature, pH and redox multi-sensitive nanogels. Reproduced with permission from reference (Qiao et al. 2011)

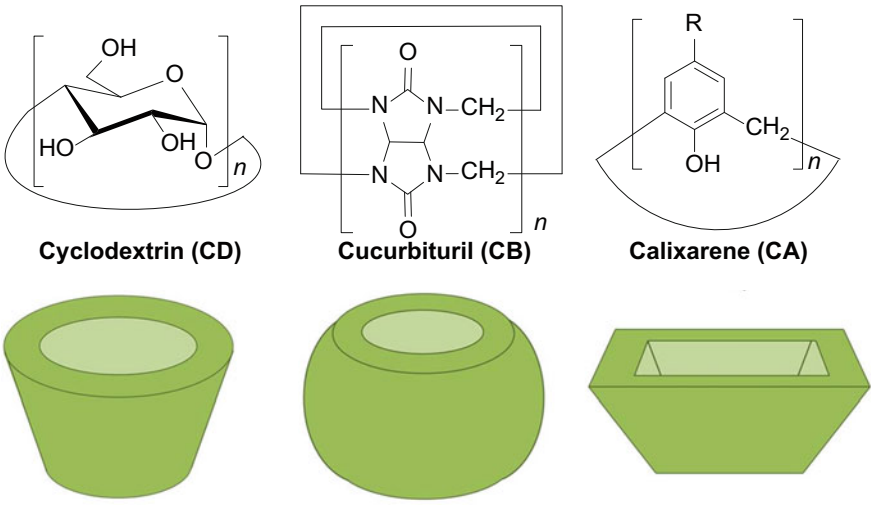

Fig. 3.3 Chemical structures and schematic representations of CD, CB, and CA. Reproduced with permission from reference (Ma and Zhao 2015)

shape or size matching, hydrophobic interaction, electrostatic interaction, or hydrogen-bonding interaction. Due to good biocompatibility of macrocyclic molecules as well as reversibility and stability of host-guest complexes, supramolecular nanosystems have been widely investigated for applications in biomedicine (Tu et al. 2011; Li et al. 2012a, b; Liu et al. 2013).

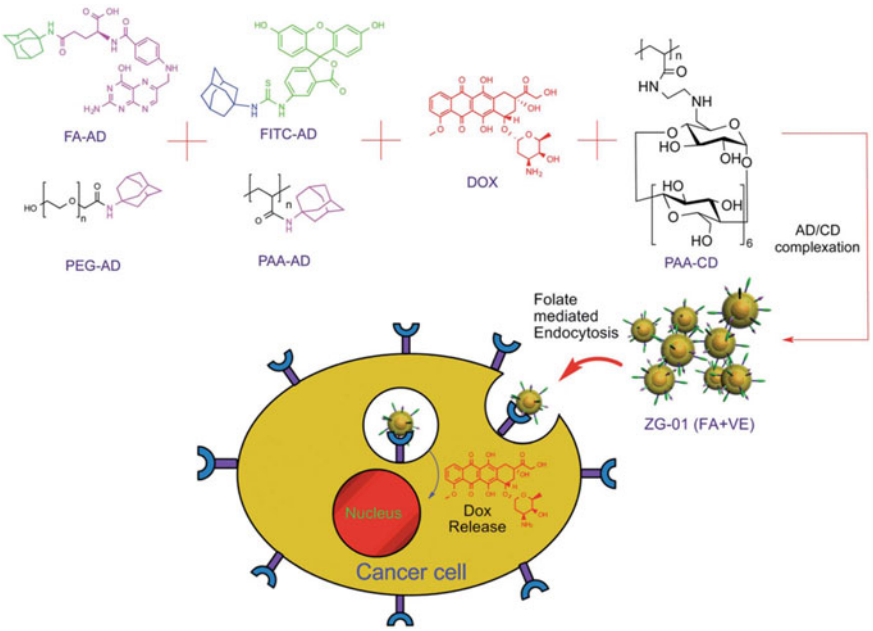

Fig. 3.4 Schematic illustration of multifunctional supramolecular nanoparticles prepared from PAA-CD, PAA-Ad, PEG-Ad, FA-Ad, and FITC-Ad for target-specific drug delivery. Reproduced with permission from reference (Ang et al. 2014a)

Ang et al. (2014a) developed multifunctional supramolecular nanoparticles through the host-guest interaction between β-CD and amantadine (Ad) (Fig. 3.4). The supramolecular nanoparticles fabricated from β-CD functionalized poly(acrylic acid) (PAA-CD), Ad-functionalized PAA (PAA-Ad) and Ad-functionalized PEG (PEG-Ad) showed a uniform size of 35 nm, with anticancer drug DOX-loaded during the preparation. Through introducing Ad-functionalized folic acid (FA-Ad) and Ad-functionalized fluorescein isothiocyanate (FITC-Ad), the synthesized supramolecular nanoparticles possessed the ability of active targeting and fluorescent bioimaging, leading to selective and efficient therapeutic efficiency toward B16F10 skin cancer cells and MDA-MB-231 breast cancer cells, and good inhibitive effects for tumor growth in vivo.

Guo et al. (2012) fabricated an enzyme sensitive supramolecular vesicle based on the host-guest interaction between *p*-sulfonatocalix[4]arene and myristoylcholine (Fig. 3.5). The supramolecular vesicle could load drug tacrine to treat Alzheimer's disease, and disassemble and release the loaded drugs upon the responsiveness to cholinesterase to destroy the hydrophilic-hydrophobic balance. Similarly, by utilizing other macrocyclic hosts, Duan et al. (2013) synthesized a novel supramolecular vesicle with a thickness of 7 nm based on host-guest interaction between hydrophilic pillar[6]arene (WP6) and hydrophobic ferrocene derivative (Fig. 3.6). This supramolecular vesicle could encapsulate anticancer drug

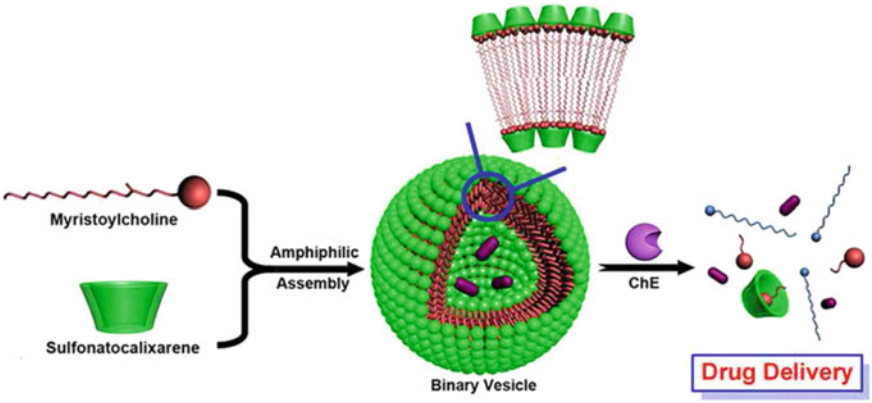

Fig. 3.5 Schematic illustration of enzyme sensitive supramolecular vesicle based on *p*-sulfonatocalix[4]arene and myristoylcholine for the delivery of tacrine to treat Alzheimer's disease. Reproduced with permission from reference (Guo et al. 2012)

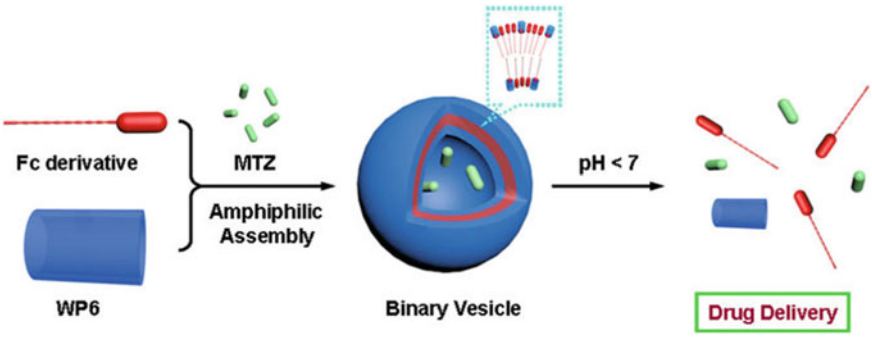

Fig. 3.6 Schematic illustration of pH-sensitive supramolecular vesicle based on WP6 and ferrocene (Fc) derivative for the delivery of anticancer drug MTZ. Reproduced with permission from reference (Duan et al. 2013)

mitoxantrone (MTZ) inside and release it under acidic pH condition, resulting in low toxicity to normal cells and comparable anticancer efficiency as free MTZ to cancer cells.

3.2.4 Others

Besides FDA-approved liposomes, polymer-based nanoparticles and supramolecular nanosystems described above, other organic nanomaterials such as conjugated polymers were also developed in recent years for application in the cancer treatment

(Xu et al. 2014). The conjugated polymers, including poly(3,4-ethylenedioxythiophene):poly(4-styrenesulfonate) (PEDOT:PSS), polyaniline, and polypyrrole (PPy) have excellent photostability and good biocompatibility, which endow them the ability to serve as therapeutic agents or multifunctional drug nanocarriers for potential combined cancer therapy (Song et al. 2014a).

Yang et al. (2011) synthesized polyoxyethylene-sterate coated polyaniline nanoparticles in the emeraldine base (EB) state (EB-PANPs) through the emulsification method for photothermal therapy (Fig. 3.7). Under the intracellular conditions, such as alkali ions, protons, or oxidative species EB-PANPs could transit to emeraldine salt (ES-PANPs) with high absorbance in near-infrared (NIR) region. With NIR irradiation, ES-PANPs had greater temperature rise than EB-PANPs or pure water. Moreover, EB-PANPs showed efficient tumor ablation both in vitro and in vivo upon exposure to 808 nm NIR laser for 5 min with a power density of 2.45 W cm^{-2}. Cheng et al. (2012a) prepared PEGylated PEDOT:PSS (PEDOT:PSS-PEG) nanoparticles through layer-by-layer (LBL) assembly for photothermal therapy (Fig. 3.8). PEDOT:PSS-PEG nanoparticles had an extended blood circulation half-life of 21.4 ± 3.1 h and high tumor accumulation efficiency of 28.02% injected dose per gram at 48 h postinjection. Furthermore, 4T1 tumors in mice could be completely eliminated at a day after intravenous injection of PEDOT:PSS-PEG nanoparticles and followed by 808 nm NIR laser irradiation for 5 min with a power density of 0.5 W cm^{-2}. Wang et al. (2013a) fabricated multifunctional PEGylated Fe_3O_4@PPy (Fe_3O_4@PPy-PEG) nanoparticles for imaging-guided and combined cancer treatment (Fig. 3.9). In this platform, Fe_3O_4 nanoparticles were used for magnetic resonance imaging and magnetic field controlled drug delivery, and PPy served as photothermal agents as well as carriers for drug loading. In vitro and in vivo experiments demonstrated that DOX-loaded Fe_3O_4@PPy-PEG possessed excellent synergistic (photothermal therapy and chemotherapy) therapeutic efficacy.

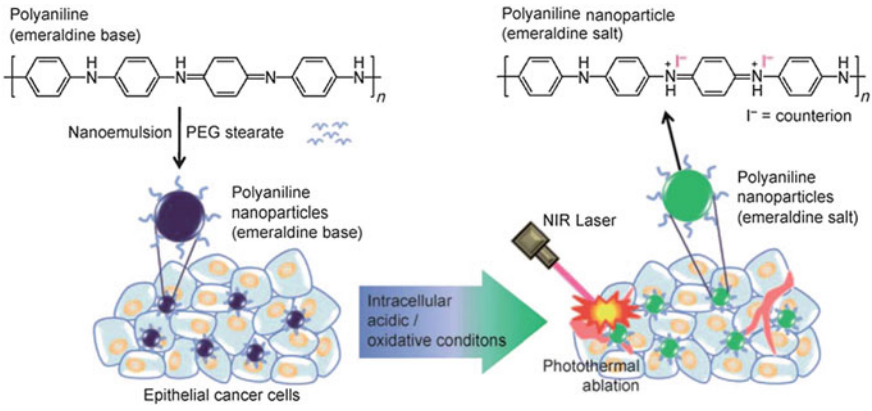

Fig. 3.7 Schematic illustration of EB-PANPs for photothermal therapy. Reproduced with permission from reference (Yang et al. 2011)

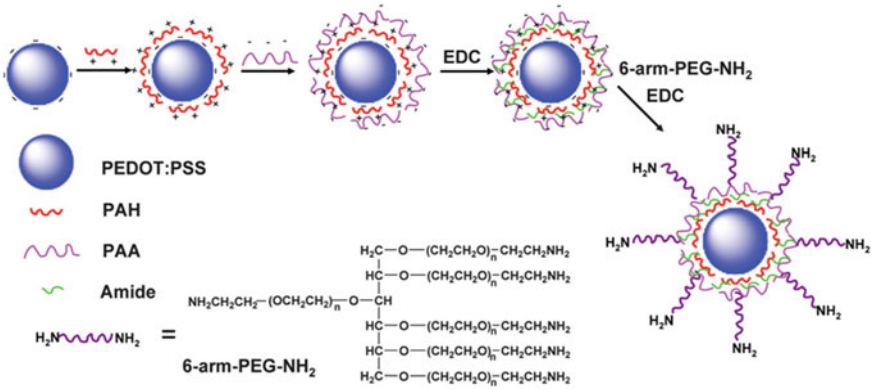

Fig. 3.8 Schematic illustration for the preparation of PEDOT:PSS-PEG nanoparticles for photothermal therapy. Reproduced with permission from reference (Cheng et al. 2012a)

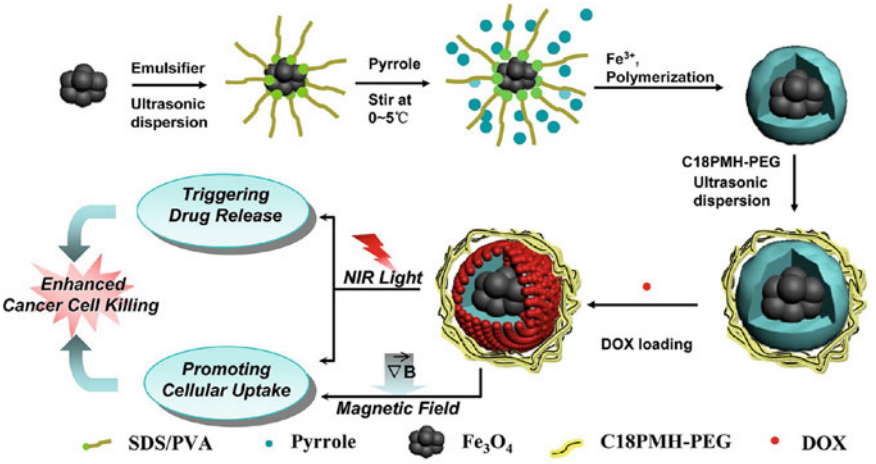

Fig. 3.9 Schematic illustration of DOX-loaded Fe_3O_4@PPy-PEG nanoparticles for imaging-guided and combined photothermal therapy and chemotherapy. Reproduced with permission from reference (Wang et al. 2013a)

3.3 Inorganic Nanomaterials

In this section, some typical inorganic nanomaterials, such as quantum dots (QDs), gold nanomaterials (gold nanoparticles and gold nanorods), mesoporous silica nanoparticles, carbon nanomaterials (carbon nanotubes, graphene, and carbon dots), upconversion nanoparticles, two-dimensional nanomaterials, and other inorganic nanoparticles are reviewed for their applications as therapeutic agents in the cancer treatment.

3.3.1 *Quantum Dots*

QDs are semiconductor nanocrystals with sizes of 2–10 nm, which consist of binary or alloyed II–VI, III–V, and IV–VI elements (Michalet et al. 2005). QDs have attracted tremendous attention from researchers worldwide based on their various distinguished properties, including (1) wide absorption spectra, (2) size-tunable, narrow, and symmetrical fluorescence spectra from ultraviolet to infrared region, and (3) high quantum yield, excellent photostability and long fluorescence lifetime. QDs can be synthesized through physical, chemical, and biological methods. Physical methods include laser irradiation of large particles and laser physical vapor deposition, but the prepared QDs have poor stability, surface defects, and low quantum yield (Jagannadham et al. 2010; Wu et al. 2015). Chemical methods consist of water-phase and organic-phase routes, which result in monodispersed QDs with excellent optical properties (Murray et al. 1993; Zhang et al. 2003). Biological methods could be used to synthesize QDs with inherent biocompatibility and biostability in mild conditions (Dameron et al. 1989; Kang et al. 2008).

Besides photovoltaics, light-emitting diodes (LEDs) and other optical applications (Shen et al. 2014; Semonin et al. 2011), QDs are also of great potential in bioimaging and drug delivery. Hong et al. (2012) prepared biocompatible 6PEG-Ag_2S QDs with emission in the second NIR region (1000–1350 nm) by coating surfactant dihydrolipoic acid (DHLA) and functionalizing amino-functional six-armed PEG on hydrophobic Ag_2S QDs, and applied it for imaging xenograft tumors in vivo (Fig. 3.10). The 6PEG-Ag_2S QDs had a long circulation half-life of about 4 h and a high tumor internalization of 10% injected dose/gram, and could be cleared via the biliary route. Muhammad et al. (2011) loaded the anticancer drug

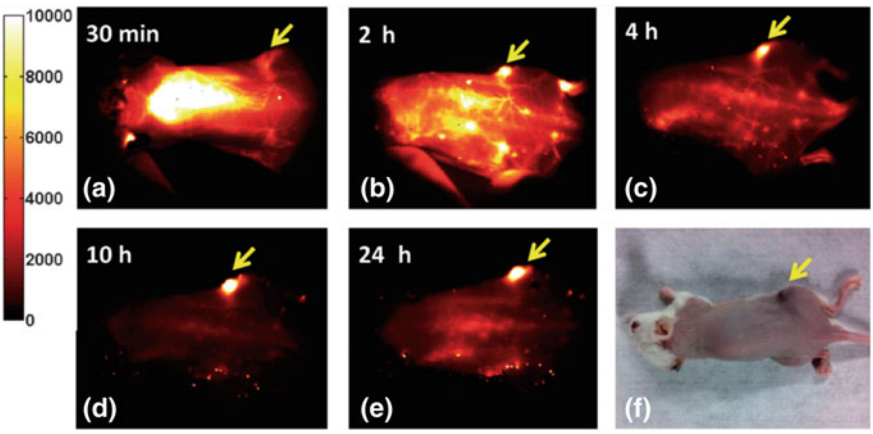

Fig. 3.10 Time-dependent NIR-II fluorescence images of 6PEG-Ag_2S QDs in vivo. Reproduced with permission from reference (Hong et al. 2012)

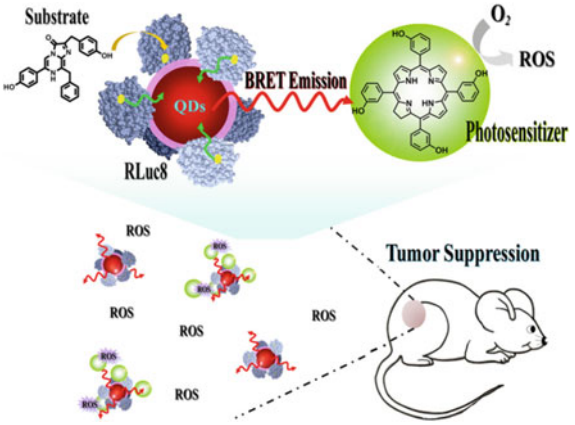

Fig. 3.11 Schematic illustration of QD-RLuc8 for photodynamic therapy. Reproduced with permission from reference (Hsu et al. 2013)

DOX and targeting ligand folic acid onto ZnO QDs. The folic acid could lead the drug nanocarrier to cancer cells and DOX was released after the degradation of ZnO QDs under acidic intracellular condition. Hsu et al. (2013) fabricated a bioluminescence resonance energy transfer (BRET) based QD-Renilla luciferase 8 (QD-RLuc8) for photodynamic therapy without external light source (Fig. 3.11). When QD-RLuc8 was exposed to coelenterazine substrate to generate RLuc8 bioluminescence, BRET could occur from RLuc8 to QD. Then the photosensitizer was activated by the energy transfer from QDs, and reactive oxygen species were generated to kill cancer cells.

However, QDs usually contain heavy metals, such as Cd, Pb, or Hg, which would induce health and environmental concerns for their biomedical applications. Therefore, biocompatible QDs without heavy metals still need to be developed for their further applications in vivo and in clinic.

3.3.2 Gold Nanomaterials

3.3.2.1 Gold Nanoparticles

Gold nanoparticles (AuNPs) are one type of Au nanostructures with size of 1.5-180 nm and localized surface plasmon resonance (LSPR) peak position from 520 to 650 nm, which are usually synthesized through reducing $HAuCl_4$ in a solution phase (Yang et al. 2015a). Taking advantage of good biocompatibility and easy functionalization, AuNPs could function as universal vehicles for bioimaging and cancer therapy. In fact, two AuNP-based therapeutics are under clinical trials with the potential to target solid tumors: Aurimmune, PEG-thiol AuNPs modified with tumor necrosis factor (TNF)-α, and AuroShell, silica nanoparticles coated with gold (Kumar et al. 2013). Till now, AuNPs have showed their versatility to ferry a

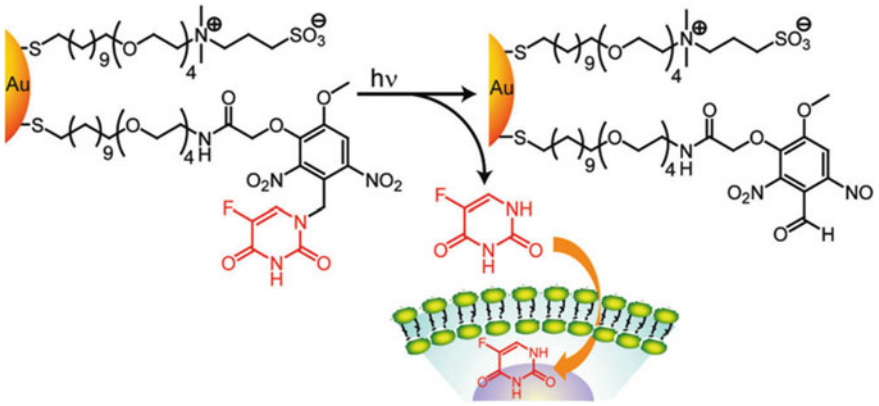

Fig. 3.12 Schematic illustration of light-mediated release of 5-FU from 5-FU loaded AuNPs. Reproduced with permission from reference (Agasti et al. 2009)

wide range of chemotherapeutic agents such as cisplatin (Kumar et al. 2014), oxaliplatin (Brown et al. 2010), kahalalide F (Hosta et al. 2009), DOX (Nam et al. 2014), 5-hydroxydecanoate (Zhuge et al. 2015), methotrexate (Chen et al. 2007), gemcitabine (Patra et al. 2010), β-lapachone (Park et al. 2009a, b), tamoxifen (Dreaden et al. 2009), 5-FU (Agasti et al. 2009), curcumin (Manju and Sreenivasan 2012), docetaxel (De Oliveira et al. 2013) and PTX (Ding et al. 2013) to cancer cells.

Agasti et al. (2009) devised an AuNP-based platform to deliver 5-FU antineoplastic agent by conjugating 5-FU to AuNPs via a photocleavable ortho-nitrobenzyl (ONB) group (Fig. 3.12). When near-UV irradiation (365 nm) was employed, 82% of 5-FU was easily cleaved from the AuNP surface. The cytotoxicity studies demonstrated that after 4 days of incubation, the viability of MCF-7 breast cancer cells declined with the increased duration of irradiation. Moreover, limited cytotoxicity was observed when the drug and light treatments were applied separately, and cytotoxicity was only observed when the drug and light treatments were administered simultaneously. Hosta et al. (2009) reported that by conjugating antitumor kahalalide F, a marine cyclodepsipeptide isolated from a mollusk, with AuNPs, selective delivery and cytotoxic activity could be enhanced. The AuNPs with various sizes (40 nm and 20 nm) were also functionalized with peptides (D-Cys or L-Cys) to introduce a positive charge, enabling better accumulation and cellular penetration in HeLa cervical cancer cells compared to the bare AuNPs. The drug and peptide conjugated AuNPs showed favored targeting to lysosomes that were the target of kahalalide F. By ligating to AuNPs of 40 nm, the cytotoxicity was enhanced as compared to the free drug due to facilitated cellular entry by AuNPs with larger size. Brown et al. (2010) reported that platinum-tethered PEGylated AuNPs could present similar or even better cytotoxicity than free oxaliplatin in various cancer cell lines (A549 lung epithelial cancer cell line and colon cancer cell lines HCT116, HCT15, HT29, RKO) and the unexpected

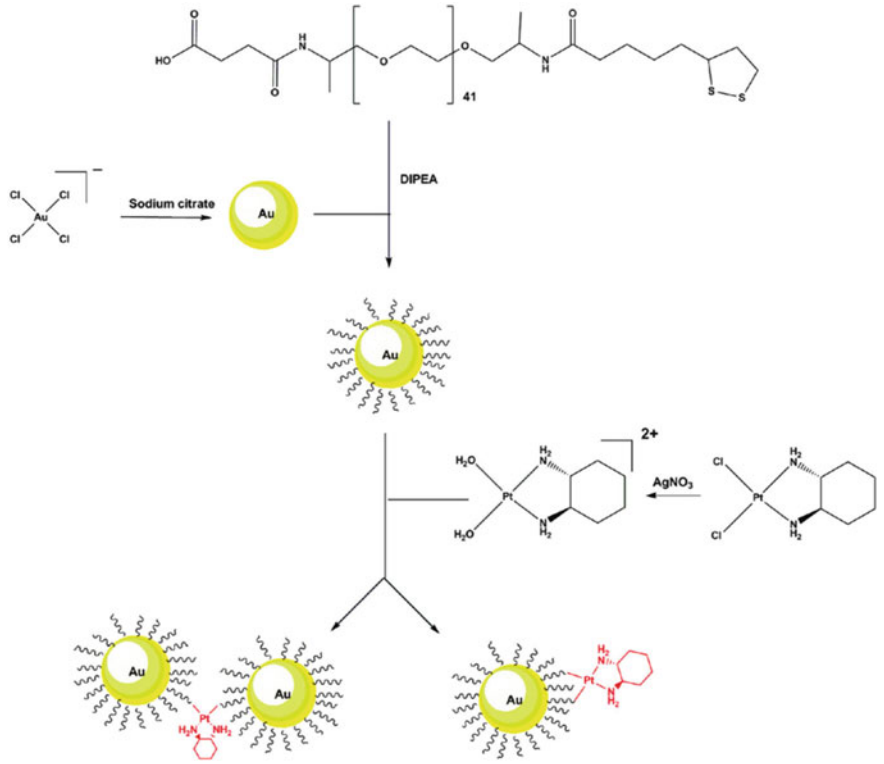

Fig. 3.13 Schematic illustration of the preparation of platinum-tethered PEGylated AuNPs for enhanced anticancer drug delivery of oxaliplatin. Reproduced with permission from reference (Brown et al. 2010)

propensity to nuclear uptake in the lung cancer cells (Fig. 3.13). In the A549 cell line, the nanodrug was about 6-fold more cytotoxic than oxaliplatin. In the colon cancer cell lines, the nanodrug was up to 5.6-fold more active or at least of similar activity as oxaliplatin.

3.3.2.2 Gold Nanorods

Gold nanorods (AuNRs) are another type of Au nanostructures with sizes from 20 nm to several μm and LSPR peak position in the range of 600–1800 nm, which could be prepared via electrochemical reduction, seed-mediated growth, photochemical reduction, bioreduction, microwave-assisted reduction or solvothermal reduction (Yang et al. 2015a). In addition to easy functionalization and excellent biocompatibility, the most celebrated property of AuNRs is the ability to trigger hyperthermia upon NIR light irradiation, depending on the aspect ratio, size and shape (Tong et al. 2007; Norman et al. 2013). Therefore, AuNRs can serve as

effective photothermal agents or as the drug nanocarriers for combination therapy (Zhang et al. 2013).

Min et al. (2010) constructed PEGylated AuNRs to deliver cisplatin. The cytotoxic effects of the conjugated AuNRs and free cisplatin were studied in three different cell lines. When compared to the free drug, the cytotoxic effect of the AuNRs-cisplatin conjugate was observed to be 9, 12, and 66-fold higher in HeLa, A549, and MCF-7 cell lines, respectively. The platinum uptake study of the AuNRs-cisplatin conjugate revealed that the platinum accumulated intracellularly was 2, 1 and 4 times higher in HeLa, A549, MCF-7 cell lines than that for cisplatin, respectively. Hence, a strong positive relationship between platinum uptake and cytotoxicity could be confirmed. Zhang et al. (2014a) fabricated a nanocomposite comprising of AuNRs@SiO_2 with pH and thermo sensitive poly (N-isopropylacrylamide-co-acrylic acid) (PNIPAM) polymer shell having lower critical solution temperature (LCST) to deliver DOX (Fig. 3.14). Sufficient temperature increase was attained after NIR laser irradiation, and at 30 min postinjection, the accumulation of the nanocomposite in heat-treated tumors showed nearly 8 times higher than the unheated tumors. In addition, more DOX was released indirectly via the nanocomposite than directly administered free DOX, regardless whether there was heating involved. The results showed that at lower temperatures, the therapeutic effect (i.e., tumor inhibition) mainly came from the chemotherapy, but at higher temperatures, the tumor regression was due to the hyperthermia effect. This platform demonstrated a novel targeted anticancer strategy without using targeting ligands for controlled and effective NIR laser-induced cancer thermochemotherapy.

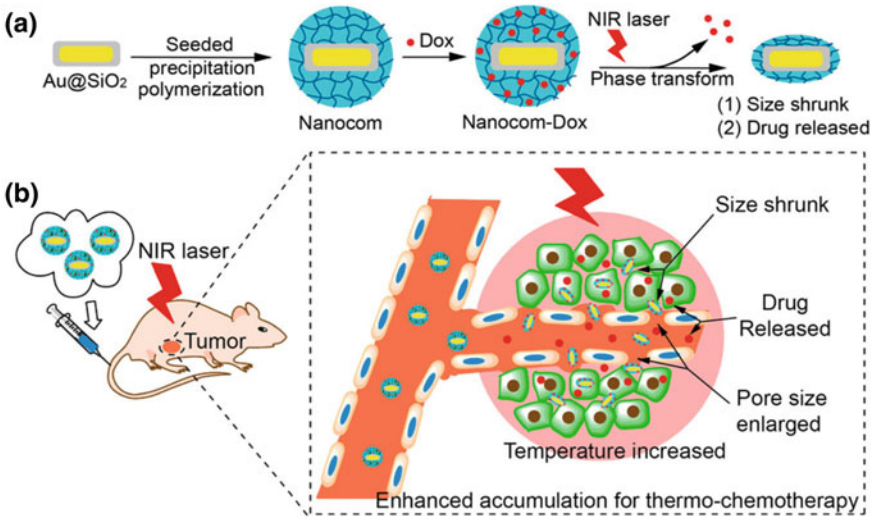

Fig. 3.14 Schematic illustration of the preparation of DOX-loaded nanocomposite (**a**) and its application for NIR laser-induced targeted thermochemotherapy (**b**). Reproduced with permission from reference (Zhang et al. 2014a)

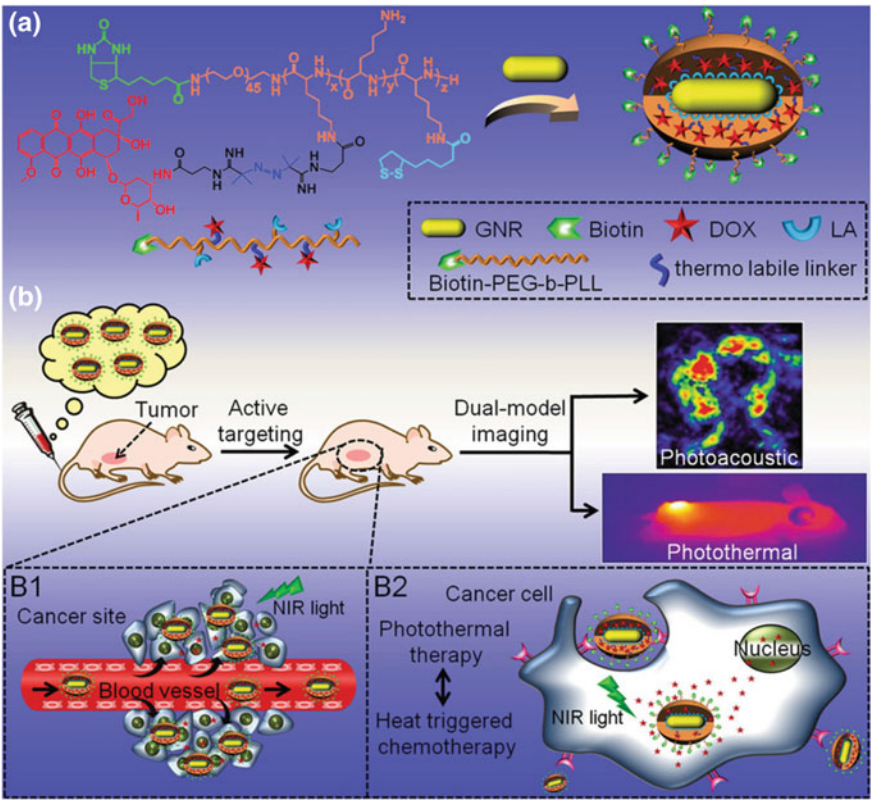

Fig. 3.15 Schematic illustration of the preparation of multifunctional AuNRs (**a**) and its application for cancer-targeted photothermal/photoacoustic imaging and thermochemotherapy (**b**). Reproduced with permission from reference (Chen et al. 2015)

Chen et al. (2015) evaluated the high potential of combined dual modalities for cancer ablation (Fig. 3.15). They coated AuNRs with a heat sensitive polyprodrug shell (Biotin-PEG-*b*-PLL(LA)-Azo-DOX). Biotin is the active targeting moiety, while the role of PEG is to avoid reticuloendothelial system (RES) elimination. Lipoic acid (LA) was conjugated to poly(L-lysine) (PLL) segment for reacting with the AuNRs, while DOX was attached onto the PLL using heat-responsive azobis(N-(2-carboxyethyl)-2-methylpropionamidine) (Azo). Upon NIR light irradiation on AuNRs to generate heat, the temperature elevation destabilized the heat unstable Azo linker and stimulated the subsequent DOX release. Off–on demand could be achieved by tuning the irradiation time and intensity of the NIR light. The in vitro cytotoxicity assays indicated that pristine AuNRs with NIR irradiation could only kill the cancer cells by thermotherapy to a limited extent, while more desired therapeutic effects were achieved by using this nanovehicle and NIR irradiation simultaneously. In addition, in vivo photothermal/photoacoustic imaging showed the high retention of the nanovehicle in the tumor, and the temperature was still

above 44.5 °C in the tumor even when using NIR illumination a day after administrating the nanovehicle. Moreover, the in vivo therapeutic efficiency could be well guided through adjusting the NIR light irradiation duration and intensity.

3.3.3 *Mesoporous Silica Nanoparticles*

Mesoporous silica nanoparticles (MSNPs) are a kind of silica materials, with pore size of 2–10 nm and three-dimensional cubic structures (Yang et al. 2012; Li et al. 2012b). The most common MSNPs are MCM-41, MCM-48 and SBA-15. MSNPs can be prepared through template-assisted method, with cetyltrimethylammonium bromide (CTAB) as the template to form the pore (Ang et al. 2014b, Fig. 3.16). During the synthesis, cylindrical assays are first formed from the CTAB micelle, followed by the controlled formation of silica walls surrounding the arrays. Then, the channels can be obtained after removing CTAB. Owing to the unique advantages of MSNPs, such as tunable pore size, large surface area, and stable mesoporous structure, MSNPs have been widely used as drug carriers to encapsulate the anticancer drugs in the mesopores for cancer therapy (Tang et al. 2012).

Yan et al. (2012) fabricated rotaxane-functionalized MSNPs for remotely photothermal-controlled curcumin release in vivo (Fig. 3.17). The controlled drug release was realized via the movement of α-CD ring upon the *cis-trans* isomerization of azobenzene axle after exposure to visible light and heat. This platform

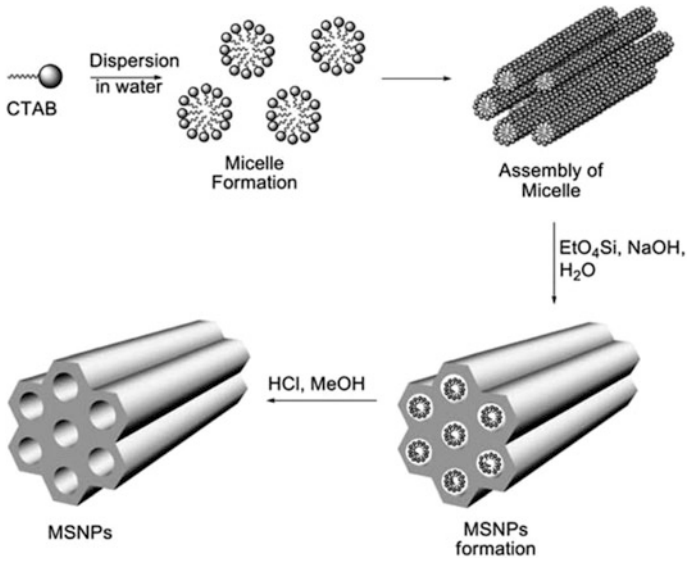

Fig. 3.16 Process for the synthesis of MSNPs *via* the template-assisted method. Reproduced with permission from reference (Ang et al. 2014b)

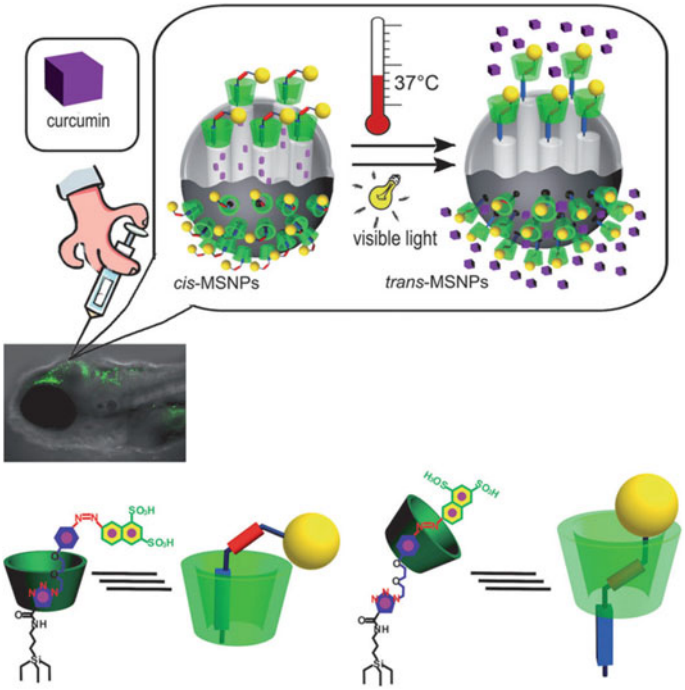

Fig. 3.17 Schematic illustration of rotaxane-functionalized MSNPs for in vivo drug delivery. Reproduced with permission from reference (Yan et al. 2012)

demonstrated effective delivery of curcumin for the treatment of heart failure on zebrafish. Ma et al. (2012) developed DOX and single strand DNA (ssDNA) co-delivered system based on MSNPs. DOX was loaded in the mesopores of MSNPs and ssDNA was complexed with the positively charged ammonium that was functionalized on MSNPs through a disulfide bond. Upon exposure to reducing agents, disulfide bond was cleaved, resulting in the release of DOX and ssDNA simultaneously. This drug nanocarrier exhibited enhanced cellular internalization and effective apoptosis of HeLa cancer cells.

Zhang et al. (2012) constructed MSNP-based targeted drug delivery system with controlled drug release behavior. DOX inside the mesopores was capped by amino-β-CD, which was bridged through disulfide bonds. Targeting ligand folic acid was introduced by adamantane and folic acid bi-functionalized PEG polymer, and the polymer was attached on the surface of MSNPs through β-CD/adamantane complexation. This developed drug nanocarrier could be internalized by HeLa cells with overexpressed folate receptor through receptor-mediated endocytosis, and realize the controlled release of DOX upon response to acidic pH in endosome and high concentration of glutathione in the cytoplasm, leading to effective inhibition of the growth of specific cancer cells. Based on the same design, Zhang et al. (2014b) synthesized MSNP-based drug carriers (PEG-MSNPs-CD-PEG-FA) with three

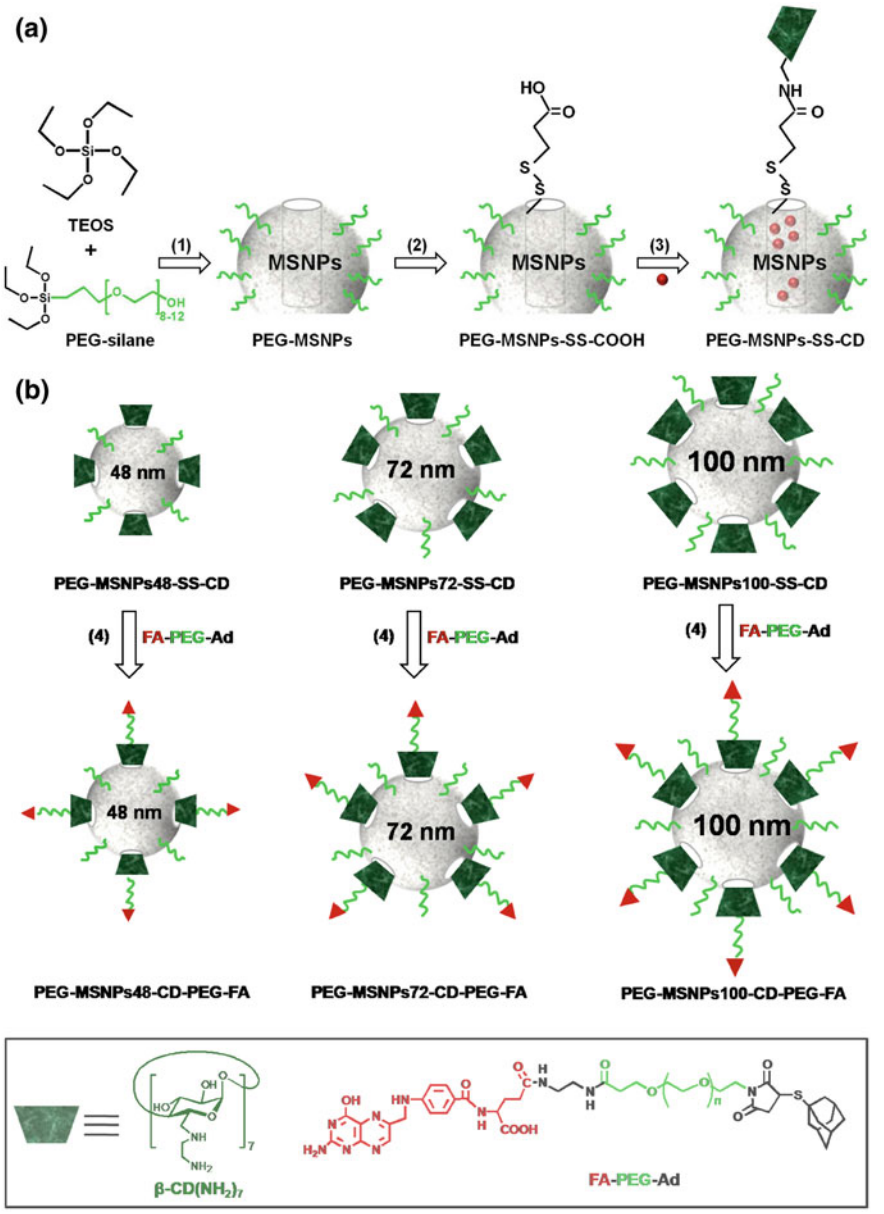

Fig. 3.18 Schematic illustration for the preparation of PEG-MSNPs-CD-PEG-FA with different sizes (48, 72, 100 nm). Reproduced with permission from reference (Zhang et al. 2014b)

different sizes (48, 72, 100 nm) for potential applications in vivo (Fig. 3.18). The results showed that the drug carrier with size of 48 nm had enhanced and selective uptake by tumor, resulting in significant tumor inhibition in mice.

3.3.4 Carbon Nanomaterials

3.3.4.1 Carbon Nanotubes

Carbon nanotubes (CNTs) were first discovered in the insoluble soot after arc burning graphite rods in 1991 (Iijima 1991). CNTs are long and tubular fullerene with hexagonal carbon in the walls and pentagonal rings in the end tips, which can be divided into two kinds, single-walled CNTs (SWCNTs), and multi-walled CNTs (MWCNTs). SWCNTs are composed by a graphite cylinder with a rolled-up single layer, and have a tube diameter of 0.4–2 nm. MWCNTs comprise of graphite sheets with multiple concentric cylindrical shells, and have an interlayer distance of about 0.36 nm and the diameters of 2–100 nm (Reilly 2007). SWCNTs and MWCNTs can be prepared by different methods, including carbon arc discharge, chemical vapor deposition, laser ablation, and pyrolysis (Karimi et al. 2015). CNTs are a kind of promising materials because of their ultralight weight, high surface area, high aspect ratio, excellent electronic and thermal properties, great chemical stability and good mechanical strength, and were applied in various fields ever since, including energy storage devices, microelectronics, nanoprobes and nanomedicine (Hong et al. 2015).

CNTs have various intriguing advantages to serve as drug carriers (Sun et al. 2014). First, CNTs can make use of EPR effect to accumulate effectively in the tumor tissues. Second, CNTs have needle-like shape, which could promote the penetration across the cellular membrane and accumulation inside cancer cells through the "nanoneedle" mechanism regardless of cell types or CNT functionalization. Besides, CNTs can also be internalized by cells through energy-dependent endocytic pathways. Third, CNTs possess high surface areas and aspect ratios, which endow them the excellent ability to load drugs on the surface or inside the core of CNTs. Importantly, targeting moieties, e.g., folic acid, RGD peptide, antibodies, aptamers, or magnetic nanoparticles, can be integrated with CNTs to offer active targeting via receptor-mediated endocytosis or external magnetic field induction. Benefited from the NIR absorption property of CNTs, CNTs can be used for photothermal therapy and even multimodal therapy by the integration with other therapeutic agents in the cancer treatment. However, before using CNTs as drug nanocarriers, some disadvantages of CNTs need to be overcome. (1) Residual metal catalysts. The remaining iron and nickel metals in the synthesized CNTs could produce free radicals in cells to cause obvious cytotoxicity, as confirmed by cell experiments. To remove residual metals, CNTs can be dispersed in mixed acids with refluxing. (2) CNT length. The length of CNTs is usually in the range from several to tens of micrometers, while studies have found that CNTs with length less than 200 nm are easier to accumulate inside cells. To truncate CNTs into short pieces, CNTs should be purified via multiple filtering. (3) Hydrophobic surface. Due to the low solubility of pristine CNTs in aqueous solution originated from highly hydrophobic surfaces, noncovalent or covalent coating methods have been developed to functionalize CNTs with suitable surface groups (PEG, polysaccharides or other hydrophilic polymers) to

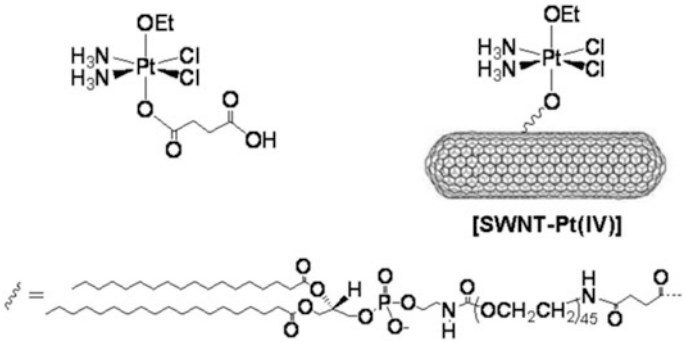

Fig. 3.19 Schematic illustration of covalently attached platinum (IV) prodrug on SWNTs. Reproduced with permission from reference (Feazell et al. 2007)

offer CNTs with water solubility and biocompatibility. Noncovalent functionalization coats CNTs with amphiphilic compounds by hydrophobic interaction (e.g., π–π interaction) and covalent functionalization is realized by amidation and esterification of oxidized CNTs or cycloaddition reactions on the side walls of CNTs.

So far, many drug delivery systems based on water-soluble CNTs have been fabricated, and drugs can be loaded on functionalized CNTs via both noncovalent and covalent linkage. Lay et al. (2010) modified CNTs with PEG-NH_2 via covalent bond and adsorbed anticancer drug PTX onto the surface. Owning to the increased solubility of PTX, the fabricated PEG-CNT-PTX showed enhanced cytotoxicity toward HeLa cells and MCF-7 cells. Feazell et al. (2007) utilized hydrophilic group modified CNTs for loading platinum (IV) via covalent bond (Fig. 3.19). The developed Pt(IV)-SWNT drug nanocarriers exhibited higher rates of cell death toward NTera-2 human embryonal cancer cells than cisplatin alone due to the improved cellular uptake of platinum (IV) by SWNTs. Yang et al. (2009) constructed a targeted drug delivery system based on magnetic nanoparticle modified CNTs under the utilization of external magnetic field (Fig. 3.20). PAA functionalized CNTs were first synthesized, followed by loading Fe_3O_4 magnetic nanoparticles and anticancer drug gemcitabine with a loading efficiency of 62%. Upon injecting post-subcutaneously, gemcitabine could be localized at lymph nodes with the guidance of magnetic field and could not be accumulated in other major organs, while gemcitabine alone did not show preferential accumulation in lymphatic system.

3.3.4.2 Graphene

Graphene is a two-dimensional single layer consisting of sp^2 hybridized carbon atoms with promising thermal, mechanical, and electrical properties, which was discovered by Geim and coworkers in 2004 and awarded Noble Prize in Physics in

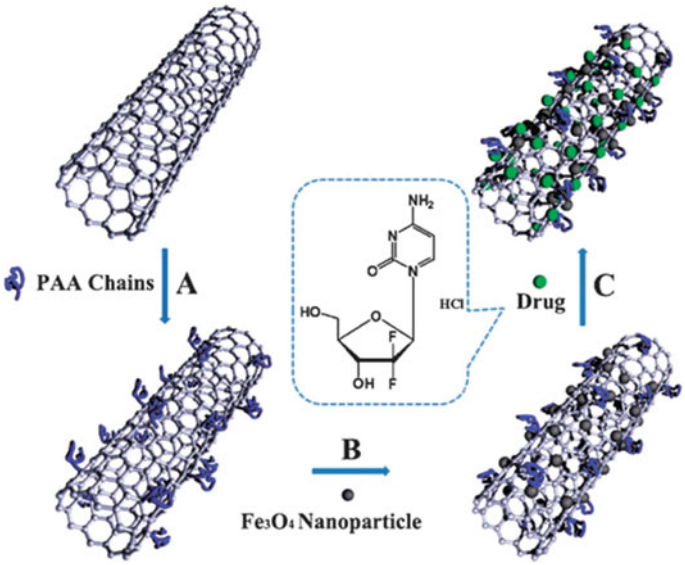

Fig. 3.20 Schematic illustration of the preparation of hydrophilic CNTs decorated with Fe_3O_4 magnetic nanoparticles and gemcitabine for magnetic field-guided drug delivery. Reproduced with permission from reference (Yang et al. 2009)

2010 (Novoselov et al. 2004, 2005). Graphene can be divided into several categories including single layer graphene, bilayer graphene, multilayer graphene, graphene oxide (GO), and reduced graphene oxide (rGO) based on the number of layers or the chemical modifications. Single layer graphene can be prepared by chemical vapor deposition or repeated mechanical exfoliation, but it is not easy to prepare single layer graphene without defect in bulk (Sprinkle et al. 2010; Novoselov et al. 2004). Owning to highly reactive surface, single layer graphene is also hard to isolate in gas phase and suspend in solutions, which limits its application in biomedicine. GO is a chemically modified graphene with high oxidation. Multilayered GO can be synthesized through rough oxidation of graphite and dispersed in aqueous solution via sonication or other methods. After repeated processing, centrifugation, and harsh treatment, monolayer oxidized graphene could be produced. GO has an amphiphilic structure with carboxylate, epoxide and hydroxyl groups and free π electrons in the plane, providing colloidal stability and the ability for drug loading through noncovalent or covalent functionalization (Park et al. 2009a; Kim et al. 2010; Guo et al. 2011). rGO is synthesized through chemical, thermal or UV processing of GO with hydrazine or other reducing molecules in order to reduce the hydrophilicity, oxygen content and surface charge, and restore the optical absorbance and electrical conductivity in GO (Park et al. 2009b; Bagri et al. 2010).

After functionalizing with small molecules, polymers or nanoparticles, graphene could be utilized as drug nanocarriers for cancer therapy. Liu et al. (2008)

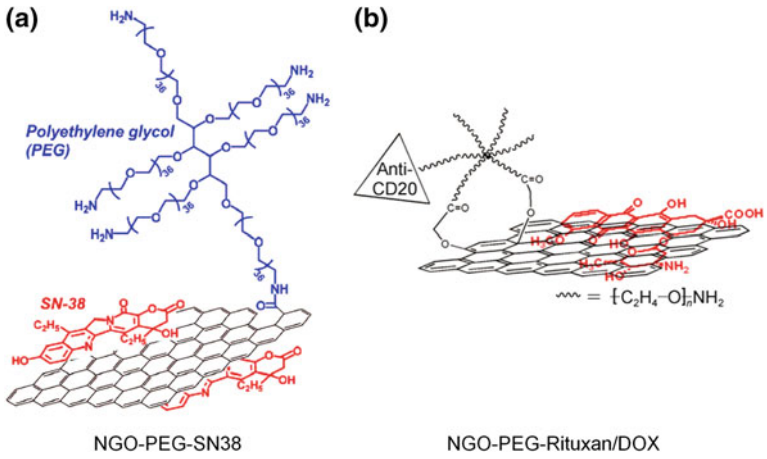

Fig. 3.21 **a** Schematic illustration of SN38 loaded NGO-PEG (NGO-PEG-SN38). Reproduced with permission from reference (Liu et al. 2008). **b** Schematic illustration of DOX-loaded NGO-PEG-Rituxan (NGO-PEG-Rituxan/DOX). Reproduced with permission from reference (Sun et al. 2008)

functionalized nanoscale GO with PEG polymer, followed by loading with a camptothecin analog SN38 by noncovalent interaction to prepare NGO-PEG-SN38 hybrid (Fig. 3.21a). This hybrid not only maintained the therapeutic efficiency of SN38, but also offered good solubility in water. In vitro experimental results showed that NGO-PEG-SN38 exhibited high toxicity toward HCT-116 cells, which was about 1000 times more efficient than camptothecin. Sun et al. (2008) developed a targeted drug delivery system based on nano-GO by conjugating rituxan (CD20+ antibody) and loading DOX through π–π stacking interaction onto PEG-NGO (Fig. 3.21b). The obtained hybrid showed pH-dependent drug release behavior in vitro. Kim et al. (2013) loaded DOX onto branched polyethylenimine (BPEI) and PEG bi-functionalized rGO (PEG-BPEI-rGO) (Fig. 3.22), and the fabricated PEG-BPEI-rGO/DOX complex could escape from endosomes through proton sponge effect and photothermally-induced endosomal disruption. Upon DOX release from the PEG-BPEI-rGO/DOX complex into cytosol by photothermal effect and glutathione, higher cytotoxicity toward cancer cells was observed with NIR irradiation when compared with those without NIR irradiation. Wu et al. (2012) loaded adriamycin (ADR) onto GO by physical mixing in order to overcome the drug resistance in DOX-resistant MCF-7/ADR cells. The fabricated drug nanocarriers (ADR-GO) had a high DOX loading amount of 93.6% and could release DOX under acidic intracellular environment. Benefited from the enhanced DOX internalization inside cancer cells by GO, ADR-GO exhibited higher therapeutic efficiency toward MCF-7/ADR cells than free drug. The above studies indicate that graphene and its derivatives possess significant applications in nanomedicine for the cancer treatment.

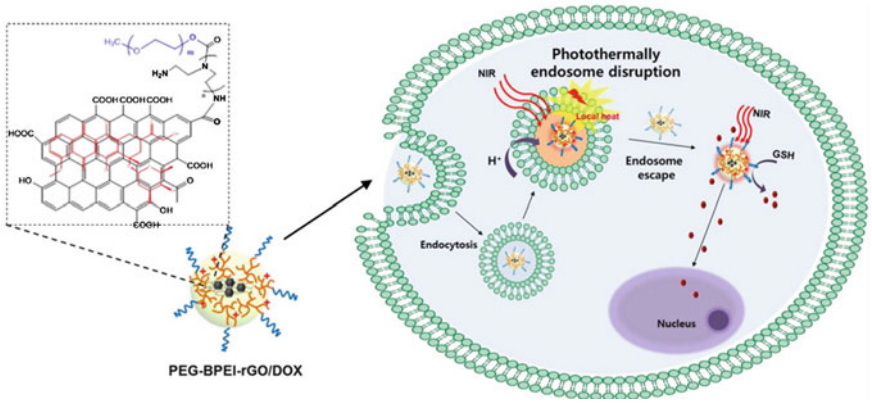

Fig. 3.22 Schematic illustration of DOX stacking onto BPEI and PEG bi-functionalized rGO (PEG-BPEI-rGO/DOX). Reproduced with permission from reference (Kim et al. 2013)

3.3.4.3 Carbon Dots

Carbon dots are another kind of carbon materials with size less than 10 nm, which were first prepared through electrophoretic purification of single-walled carbon nanotubes (Xu et al. 2004). Until now, different methods have been developed for the synthesis of carbon dots, including top-down methods and bottom-up methods (Song et al. 2014b). For top-down synthesis, different approaches such as laser ablation, arc discharge, nitric acid/sulfuric acid oxidation or electrochemical oxidation can be used to break down the carbon structure of amorphous carbon (carbon black and candle soot) and regular sp^2 carbon layers (carbon nanotubes and graphite rod) (Peng and Travas-Sejdic 2009; Deng et al. 2014; Hu et al. 2009; Zhu et al. 2009). For bottom-up preparation, small molecules with plenty carboxyl, hydroxyl and amine groups, e.g., citric acid (Zhai et al. 2012), ascorbic acid (Jia et al. 2012), amino acid (Jiang et al. 2012), and glycerol (Liu et al. 2012a), can be regarded as the carbon precursors via hydrothermal, microwave-assisted pyrolysis and calcinations methods. Moreover, bio-products from animal hair (Sun et al. 2013), silk (Li et al. 2013; Wu et al. 2013), bovine serum albumin (Wee et al. 2013), barbecue meat (Wang et al. 2013b) and plant extracts [banana juice (De and Karak 2013), watermelon peel (Zhou et al. 2012), soy milk (Zhu et al. 2012; Krysmann et al. 2012), and grass (Liu et al. 2012b)] can also be used for the synthesis of carbon dots.

Carbon dots are also a new class of fluorescent materials with emissive wavelength from blue to near-infrared. The wide fluorescence range can be obtained by the excitation-dependent emission or different synthetic and purification methods. Carbon dots have high quantum yield and good photostability to overcome the drawbacks of photobleaching for organic dyes or photoblinking for quantum dots.

Benefited from these excellent properties, carbon dots can be utilized for bioimaging both in vitro and in vivo. Zhai et al. (2012) used citric acid and different amine molecules to prepare carbon dots with high luminescence through a microwave-assisted pyrolysis method. The amine molecules can be used as both precursors for N-doping and agents for the surface passivation. The synthesized carbon dots by citric acid and 1,2-ethylenediamine had a quantum yield of 30.2% and can be applied for labeling L929 mouse fibroblast cells with blue, green and red colors with excitation wavelengths of 405, 488, and 543 nm. Tao et al. (2012) prepared carbon dots by the oxidization of graphite or carbon nanotubes with mixed acids and proved the capability of carbon dots for NIR fluorescence imaging in vivo. The results suggested renal and fecal excretion routes for the clearance of carbon dots, and presented no noticeable in vivo toxicity through time-course blood tests and histological analysis, indicating a great potential of carbon dots as non-toxic fluorescent nanoprobes for biomedical bioimaging. Shi et al. (2014) synthesized nitrogen-doped carbon dots with a high yield of 78% via one-step hydrothermal method by using ethylenediamine tetraaceticacid as a precursor. In vivo zebrafish bioimaging results showed that green emissive carbon dots could be adsorbed by swallowing and skin, and were accumulated with tissue-dependent affinity (in the eye, yolk sac, or tail). The utilization of carbon dots in zebrafish supports their future application as low-toxic probes in clinic.

More importantly, carbon dots have also been utilized as drug nanocarriers for the delivery of chemotherapy drugs, photosensitizers and therapeutic genes for cancer therapy. Tang et al. (2013) utilized Förster resonance energy transfer (FRET)-based carbon dots to fabricate a drug delivery system (CDot-FA-DOX, Fig. 3.23). The carbon dots were synthesized through a modified electrochemical method and used as both FRET donor and drug nanocarriers. The fluorescent anticancer drug DOX was used as FRET acceptor and loaded on the surface of carbon dots by π–π stacking and electrostatic interactions. The release of DOX

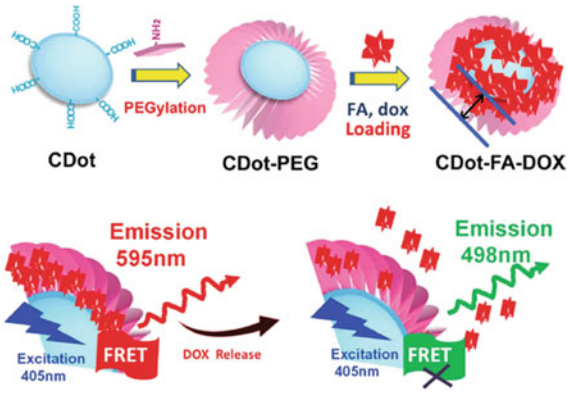

Fig. 3.23 Schematic illustration of the preparation of FRET-based CDot-FA-DOX and its mechanism for real time monitoring of DOX release. Reproduced with permission from reference (Tang et al. 2013)

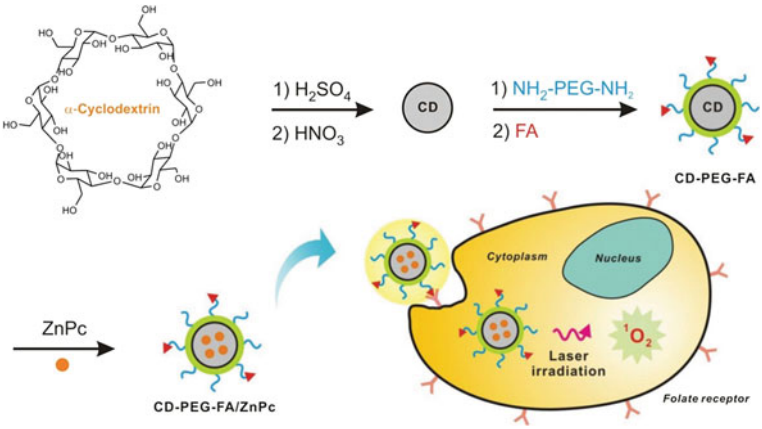

Fig. 3.24 Schematic illustration of the preparation of CD-PEG-FA/ZnPc and its application for targeted photodynamic therapy. Reproduced with permission from reference (Choi et al. 2014)

could be monitored in real time by FRET signal change upon tuning the pH of the environment. Moreover, the drug nanocarriers could also be used for two-photon imaging at tumor tissues of 65–300 μm with the excitation wavelength of 810 nm, demonstrating the possibility of carbon dots for monitoring the drug release in deep tumor tissues.

Choi et al. (2014) fabricated a folic acid (FA)-functionalized carbon dots to load photosensitizer zinc phthalocyanine (ZnPc) for simultaneous biological imaging and targeted photodynamic therapy (Fig. 3.24). The CD-PEG-FA/ZnPc hybrid was prepared by the thermal decomposition of α-cyclodextrin and functionalized with passivation agent PEG and targeting ligand FA, followed by loading ZnPc onto the surface through π-π stacking interaction. The developed drug delivery system could target cancer cells with overexpressed folate receptors and reveal targeted photodynamic therapy upon irradiation in vitro and in vivo. The system is expected to provide a convenient and effective method to enhance photodynamic therapy for the cancer treatment in future. Liu et al. (2013) used glycerol and branched PEI25k to synthesize polyethylenimine (PEI) functionalized carbon dots by one-step microwave-assisted pyrolysis, in which PEI served as both surface passivation agent for fluorescence enhancement and polyelectrolyte for condensing DNA. By optimizing the pyrolysis time, the obtained carbon dots could exhibit low toxicity and high gene expression of plasmid DNA in HepG2 human liver cancer cells and COS-7 fibroblast-like cells, with excitation wavelength-dependent fluorescent emission inside cells. These results suggest the promising applications of carbon dots in bioimaging and gene delivery.

3.3.5 *Upconversion Nanoparticles*

Lanthanide-doped upconverting nanoparticles (UCNPs) were first developed in 2000 and can convert NIR light to UV or visible light, among which hexagonal $NaYF_4$ (β-$NaYF_4$) is the commonly used inorganic host and Er^{3+}, Tm^{3+}, and Ho^{3+} ions are the popular activators for upconversion luminescence (UCL) generation with the excitation wavelength of 800 nm or 980 nm (Fig. 3.25, Haase and Schaefer 2011; Wu and Butt 2016). UCNPs could be synthesized through hydro-/solvothermal method, thermal decomposition method, coprecipitation method, microemulsion method, sol-gel process, ionic-liquid-based method, and microwave-assisted method (Gai et al. 2014). Benefited from the advantages of NIR excitation, including negligible photodamage and deep tissue penetration, UCNPs can serve as promising materials for deep tissue biomedical applications including UCL bioimaging, photodynamic therapy, photothermal therapy, and UCNP-assisted photolysis for drug activation (Dong et al. 2015).

Idris et al. (2012) co-loaded merocyanine 540 (MC540) and zinc phthalocyanine (ZnPc) into $NaYF_4$:Yb,Er@$mSiO_2$ to afford UCNs-ZnPc-MC540, in which the absorption peaks of MC540 and ZnPc overlap with the green and red emission

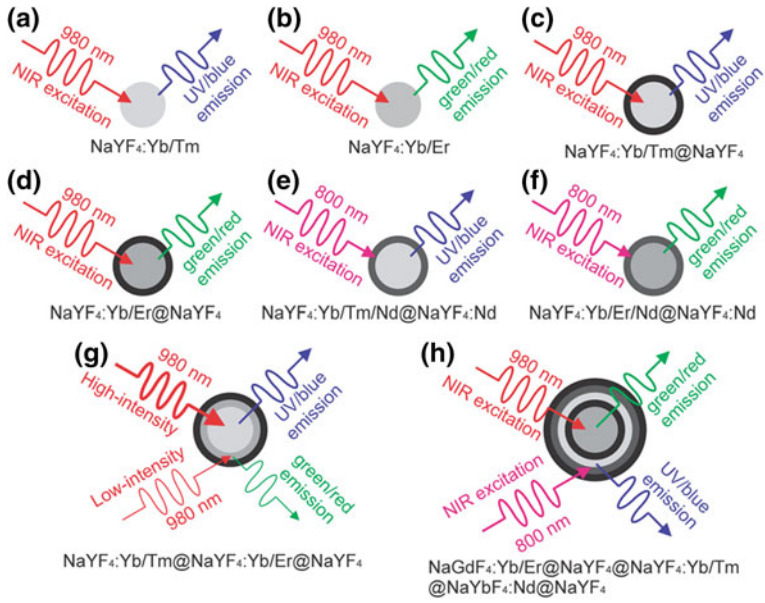

Fig. 3.25 Schematic illustration of different UCNPs. Reproduced with permission from reference (Wu and Butt 2016)

peaks of $NaYF_4$:Yb,Er UCNPs. The two photosensitizer-loaded UCNs-ZnPc-MC540 exhibited increased singlet oxygen generation and enhanced cell-killing efficiency with irradiation of 980 nm laser, when compared with single photosensitizer-loaded UCNPs. Moreover, when UCNs-ZnPc-MC540 was injected to the tumor-bearing mice and irradiated with an NIR laser of 980 nm, the inhibition of tumor growth in vivo was achieved, while no obvious influence was observed when the tumor-bearing mice was treated with radiation or $NaYF_4$:Yb, Er@$mSiO_2$ alone. In addition, more efficient antitumor results were realized when UCNs-ZnPc-MC540 was further conjugated with active targeting ligands (folic acid or antibody) as compared with unmodified UCNs-ZnPc-MC540.

Cheng et al. (2012b) developed a multifunctional nanoparticle $NaYF_4$:Yb, Er@Fe_3O_4@Au-PEG for UCL/MRI dual-modal imaging and magnetically targeted photothermal therapy (Fig. 3.26). When $NaYF_4$:Yb,Er@Fe_3O_4@Au-PEG was injected intravenously in vivo and the tumor was attached on a magnet, UCL signal increased by several folds and T2-weighted MRI signals decreased by 62.1%. Moreover, when the tumor was irradiated with an NIR laser of 808 nm, an increased surface temperature (about 50 °C) was achieved under the magnetic field, resulting in the disappearance of all the tumors. No obvious temperature change was observed (about 38 °C) for the tumors without the injection of $NaYF_4$:Yb, Er@Fe_3O_4@Au-PEG. The results exhibited a prominent therapeutic efficiency with 100% elimination of tumors. Ma et al. (2013) designed a multifunctional UCNPs/polymer composite UCNP@P-Pt/RhB for up/down-conversion bioimaging in vitro and ex/in vivo and the delivery of cisplatin (IV) drug. The UCNP@P-Pt/RhB could release cytotoxic cisplatin inside the reductive intracellular

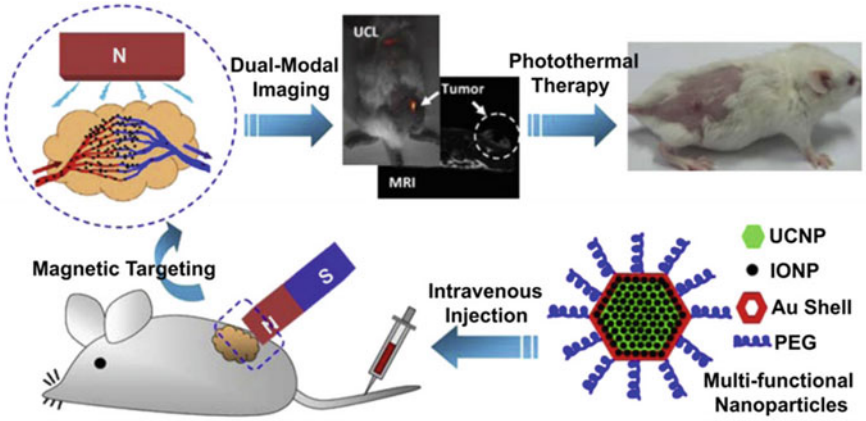

Fig. 3.26 Schematic illustration of $NaYF_4$:Yb,Er@Fe_3O_4@Au-PEG nanoparticle for dual-modal imaging and magnetically targeted photothermal therapy. Reproduced with permission from reference (Cheng et al. 2012b)

condition or tumor-bearing animal models, and could regulate the apoptotic genes for promoting the apoptosis of tumor cells. This system highlights the mechanism for the antitumor effects of cisplatin (IV) drug and the potential application of UCNP@P-Pt/RhB for the cancer treatment.

3.3.6 *Two-Dimensional Nanomaterials*

In addition to graphene, various two-dimensional nanomaterials with excellent physical and chemical properties have received tremendous attention in recent years, which include ultrathin transition metal dichalcogenides (TMDCs) and black phosphorus nanosheets (Zhang 2015). TMDCs, consisting of MoS_2, $MoSe_2$, WS_2, or WSe_2 are semiconductors with bandgaps within 1–2 eV for their ultrathin layers (Lu et al. 2016). Black phosphorus is a semiconductor, with thickness-dependent bandgap from 2.0 eV for single layer to 0.3 eV for bulk (Tran et al. 2014). These two-dimensional nanomaterials not only possess promising applications in electronic and optoelectronic devices, but also reveal fantastic potentials in biological fields (Kalantar-zadeh et al. 2015; Sun et al. 2015).

Liu et al. (2014) developed a multifunctional drug carrier based on MoS_2 nanosheets for combined cancer therapy (Fig. 3.27). MoS_2 nanosheets were prepared via chemical exfoliation method from the bulk materials followed by the functionalization with lipoic acid modified PEG (LA-PEG) through a thiol reaction to offer the physiological stability and biocompatibility. Owning to strong NIR absorbance and extraordinary surface-area-to-mass ratio, MoS_2-PEG nanosheets could serve as promising photothermal agents as well as the nanocarriers to load therapeutic molecules such as a photodynamic agent chlorine e6 (Ce6) or anticancer drugs 7-ethyl-10-hydroxycamptothecin (SN38) and DOX. Furthermore, combined

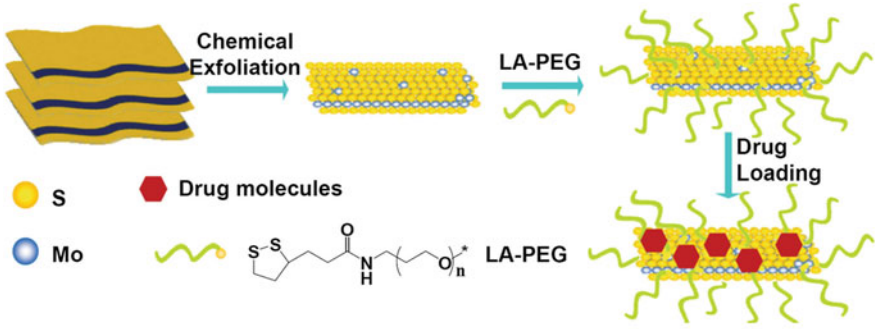

Fig. 3.27 Schematic illustration of the preparation of DOX-loaded MoS_2-PEG for combined photothermal and chemotherapy. Reproduced with permission from reference (Liu et al. 2014)

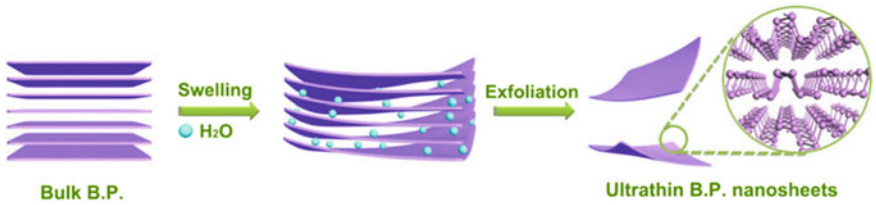

Fig. 3.28 Schematic illustration of the preparation of exfoliated black phosphorus (B.P.) nanosheets for photodynamic therapy. Reproduced with permission from reference (Wang et al. 2015)

photothermal and chemotherapy could be achieved both in vitro and in vivo for the DOX-loaded MoS_2-PEG, revealing the great potential of two-dimensional TMDCs as novel drug nanocarriers for combined cancer treatment. Wang et al. (2015) illustrated that the exfoliated black phosphorus nanosheets could serve as effective photosensitizers to generate singlet oxygen with a high quantum yield of about 0.91 for the application in photodynamic therapy (Fig. 3.28). These black phosphorus nanosheets could inhibit the growth of cells/tumor effectively with a small amount and short light irradiation both in vitro and in vivo. Compared with other metal-free photosensitizers, the black phosphorus nanosheets could undergo ready degradation into biocompatible phosphorus oxides under light irradiation without any residual, which offer a great therapeutic potential for the cancer therapy. This study could provide a novel insight into the extensive application of black phosphorus.

3.3.7 Others

Besides quantum dots, gold nanomaterials, mesoporous silica nanoparticles, carbon nanomaterials, upconversion nanoparticles, and two-dimensional nanomaterials described above, other inorganic nanomaterials, such as CuS, Bi_2S_3, and FeS, were also developed in recent years for applications in cancer therapy (Tian et al. 2011; Ai et al. 2011; Yang et al. 2015b). These new inorganic nanomaterials not only serve as the drug carriers to deliver chemo-drugs, photosensitizers or photothermal agents, but also possess the ability for bioimaging or acting as therapeutic agents themselves, which could provide new insights to develop potential therapeutic agents for imaging-guided and combined cancer treatment in clinic.

Tian et al. (2011) synthesized hydrophilic flower-like CuS superstructures for effective photothermal therapy under the excitation of 980 nm (Fig. 3.29). Compared with corresponding building blocks (hexagonal nanoplates), CuS superstructures could enhance the magnitude of NIR photothermal conversion efficiency by approximate 50%. Upon 980 nm laser irradiation with a power density of 0.51 W cm^{-2}, the temperature of CuS superstructure aqueous solution could increase by 17.3 °C in 5 min. Moreover, these CuS superstructures could

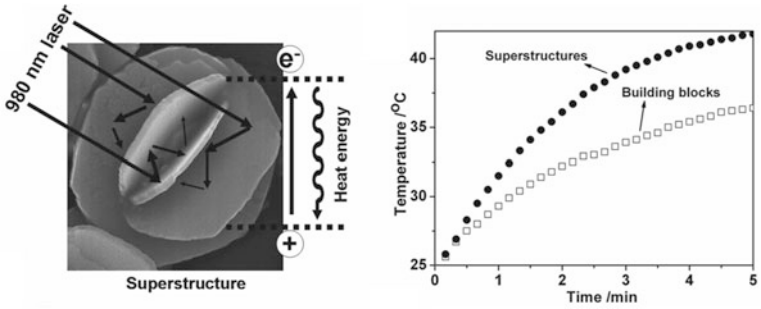

Fig. 3.29 Schematic illustration of CuS superstructures for effective photothermal therapy. Reproduced with permission from reference (Tian et al. 2011)

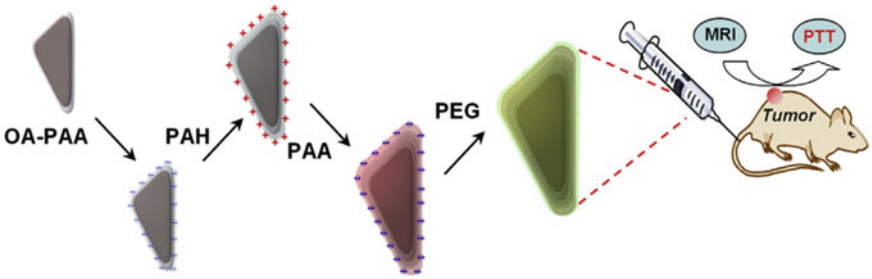

Fig. 3.30 Schematic illustration of PEGylated FeS nanoplates for magnetic resonance imaging-guided photothermal therapy. Reproduced with permission from reference (Yang et al. 2015b)

ablate cancer cells in vivo effectively by their photothermal effects. Yang et al. (2015b) fabricated magnetic FeS nanoplates for photothermal therapy of cancer with simultaneous magnetic resonance imaging. FeS nanoplates were prepared through a facile one-step approach and could reveal strong superparamagnetism with high NIR absorbance after the PEG functionalization (Fig. 3.30). The FeS-PEG nanoplates had much higher transverse relaxivity (r2, 209.8 mM^{-1} S^{-1}) when compared to iron oxide nanoparticles or some clinical approved T2-contrast agents, and could achieve a high accumulation in tumor after intravenous injection as confirmed by magnetic resonance imaging. Moreover, FeS-PEG nanoplates could be cleared from major organs of mice, resulting in little toxicity to the administrated animals even at a high dose (100 mg/kg). After intravenous injection of these nanoplates with a dose of 20 mg/kg and upon irradiation with 808-nm NIR laser, efficient photothermal treatment of cancer in vivo was achieved. These results showed PEGylated FeS nanoplates may serve as potential therapeutic agents for future clinical translation.

3.4 Organic–Inorganic Hybrid Nanomaterials

In recent years, organic–inorganic hybrid nanomaterials, composed of both organic and inorganic moieties through covalent or noncovalent interactions, have been employed as nanocarriers for applications in cancer therapeutics (Hood et al. 2014). Upon integrating the intrinsic physical/chemical properties of the organic and inorganic components, organic-inorganic hybrid nanomaterials can possess improved stability, multiple functionalities, and biocompatibility for the treatment of cancer more efficiently (Sreejith et al. 2015).

Wang et al. (2012) fabricated polymer-QD hybrid nanoparticles for bioimaging and chemotherapy (Fig. 3.31). The diblock copolymer folate-PEG-*b*-poly(*N*-(*N*′,*N*′-diisopropyl-aminoethyl)aspartamide)-cholic acid (FA-PEG-*b*-PAsp(DIP)-CA) with

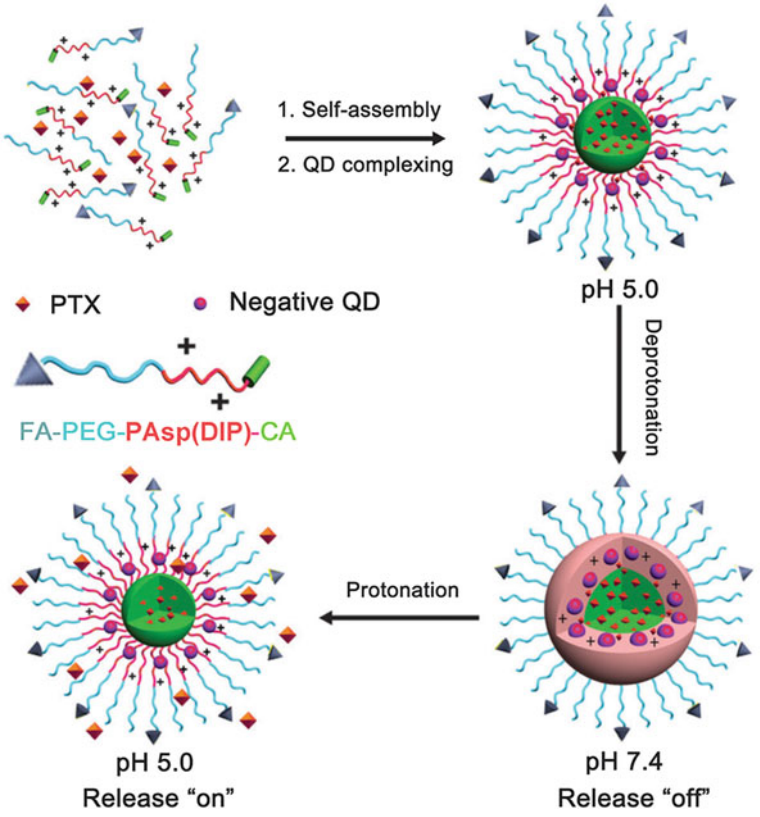

Fig. 3.31 Schematic illustration of PTX and QD loaded micelles for fluorescent imaging and pH-responsive drug release. Reproduced with permission from reference (Wang et al. 2012)

pH-sensitive moieties was synthesized and assembled into micelles in aqueous solution, with CA as the core, PAsp(DIP) as the inner shell, and PEG as the corona. The anticancer drug PTX could be loaded into the core, negatively charged quantum dots were introduced into the inner shells for fluorescent imaging, and folic acid in the coronas was used for active targeting of the cancer cells. PTX drugs were released under intracellular acidic lysosomal condition, while only few amounts of drugs were released under physiological pH. The PTX and QD loaded micelles exhibited efficient inhibition for the tumor growth in vivo.

Wang et al. (2011) developed polymer-UCNP hybrid nanoparticles for photodynamic therapy (Fig. 3.32). PEG-grafted poly(maleicanhydride-alt-1-octadecene) (C18PMH-PEG) amphiphilic polymer was functionalized onto oleic acid capped UCNPs, followed by loading photosensitizer Chlorin e6 (Ce6) through hydrophobic interaction. The formed UCNP-Ce6 could generate singlet oxygen to kill cancer cells with exposure under NIR light (980 nm). In vivo experiments demonstrated outstanding photodynamic therapeutic effects of UCNP-Ce6 toward tumor-bearing mice upon intratumoral injection and NIR light irradiation, and no obvious toxicity to the mice because of the gradual clearance of UCNP-Ce6 from the body. In another case, Luo et al. (2013) fabricated hybrid [2]rotaxane-functionalized hollow mesoporous silica nanoparticles (HMSNs) for targeted and redox-responsive chemotherapy (Fig. 3.33). Mechanically interlocked molecules ([2]rotaxanes) were anchored onto the pores of HMSNs via disulfide bonds, and folic acid served as stoppers of the [2]rotaxanes and active targeting ligands. This hybrid system showed targeted ability toward tumor tissues in vitro and controlled drug release under reductive intracellular condition, resulting in excellent therapeutic efficiency to tumors in vivo.

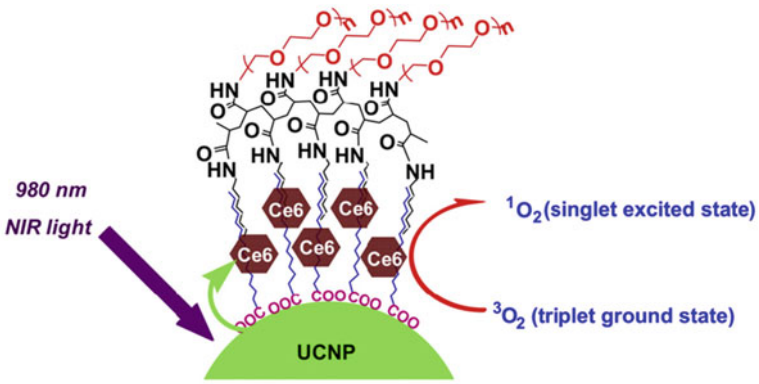

Fig. 3.32 Schematic illustration of polymer-UCNP hybrid nanoparticles for photodynamic therapy. Reproduced with permission from reference (Wang et al. 2011)

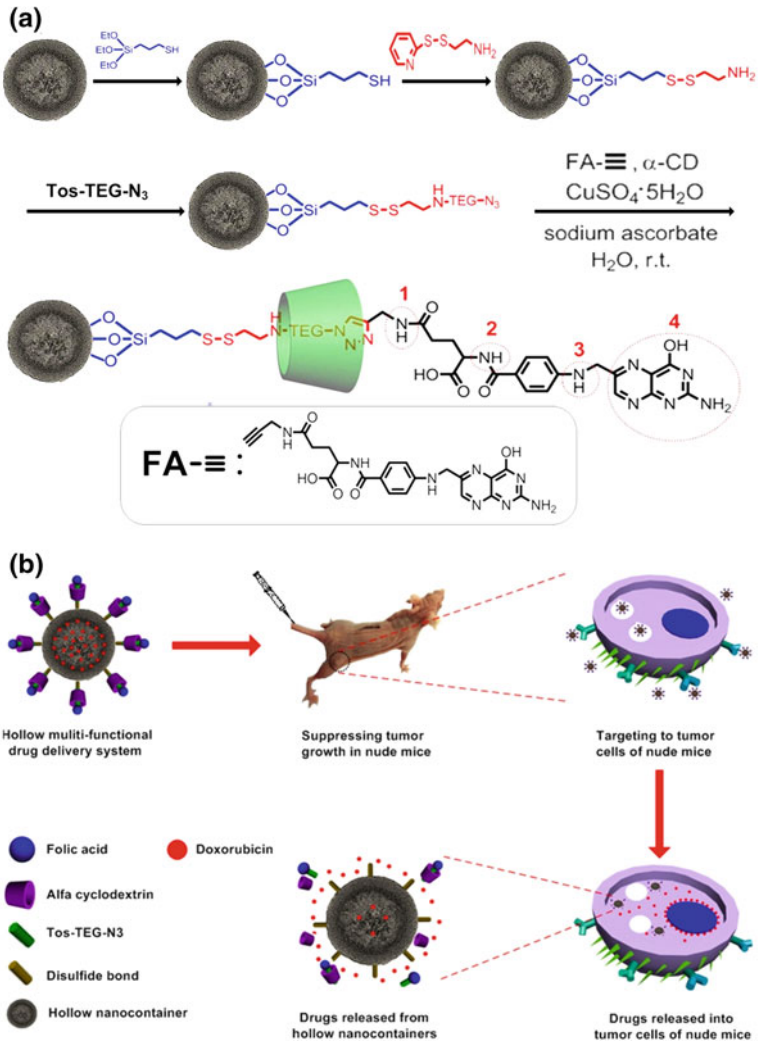

Fig. 3.33 Schematic illustration of [2]rotaxane-functionalized HMSNs for targeted and redox-responsive chemotherapy. Reproduced with permission from reference (Luo et al. 2013)

References

Agasti SS, Chompoosor A, You CC, Ghosh P, Kim CK, Rotello VM (2009) Photoregulated release of caged anticancer drugs from gold nanoparticles. J Am Chem Soc 131:5728–5729

Ai K, Liu Y, Liu J, Yuan Q, He Y, Lu L (2011) Large-scale synthesis of Bi_2S_3 nanodots as a contrast agent for in vivo X-ray computed tomography imaging. Adv Mater 23:4886–4891

Ang CY, Tan SY, Wang X, Zhang Q, Khan M, Bai L, Tamil Selvan S, Ma X, Zhu L, Nguyen KT, Tan NS, Zhao YL (2014a) Supramolecular nanoparticle carriers selfassembled from cyclodextrin and adamantine functionalized polyacrylates for tumor-targeted drug delivery. J Mater Chem B 2:1879–1890

Ang CY, Tan SY, Zhao YL (2014b) Recent advances in biocompatible nanocarriers for delivery of chemotherapeutic cargoes towards cancer therapy. Org Biomol Chem 12:4776–4806

Aw MS, Kurian M, Losic D (2013) Polymeric micelles for multidrug delivery and combination therapy. Chem Eur J 19:12586–12601

Bae Y, Nishiyama N, Kataoka K (2007) In vivo antitumor activity of the folate-conjugated pH-sensitive polymeric micelle selectively releasing adriamycin in the intracellular acidic compartments. Bioconjugate Chem 18:1131–1139

Bagri A, Mattevi C, Acik M, Chabal YJ, Chhowalla M, Shenoy VB (2010) Structural evolution during the reduction of chemically derived graphene oxide. Nat Chem 2:581–587

Barenholz Y (2012) Doxil(R)—the first FDA-approved nano-drug: lessons learned. J Control Release 160:117–134

Bedikian AY, Silverman JA, Papadopoulos NE, Kim KB, Hagey AE, Vardeleon A (2011) Pharmacokinetics and safety of marqibo (vincristine sulfate liposomes injection) in cancer patients with impaired liver function. J Clin Pharmacol 51:1205–1212

Brown SD, Nativo P, Smith JA, Stirling D, Edwards PR, Venugopal B, Flint BJ, Plumb JA, Graham D, Wheate NJ (2010) Gold nanoparticles for the improved drug delivery of the active component of oxaliplatin. J Am Chem Soc 132:4678–4684

Chen YH, Tsai CY, Huang PY, Chang MY, Cheng PC, Chou CH, Chen DH, Wang CR, Shiau AL, Wu CL (2007) Methotrexate conjugated to gold nanoparticles inhibits tumour growth in a syngeneic lung tumour model. Mol Pharm 4:713–722

Chen WH, Yang CX, Qiu WX, Luo GF, Jia HZ, Lei Q, Wang XY, Liu G, Zhuo RX, Zhang XZ (2015) Multifunctional theranostic nanoplatform for cancer combined therapy based on gold nanorods. Adv Healthcare Mater 4:2247–2259

Cheng L, Yang K, Chen Q, Liu Z (2012a) Organic stealth nanoparticles for highly effective in vivo near-infrared photothermal therapy of cancer. ACS Nano 6:5605–5613

Cheng L, Yang K, Li Y, Zeng X, Shao M, Lee ST, Liu Z (2012b) Multifunctional nanoparticles for upconversion luminescence/MR multimodal imaging and magnetically targeted photothermal therapy. Biomaterials 33:2215–2222

Cheng R, Meng FH, Deng C, Klok HA, Zhong ZY (2013) Dual and multi-stimuli responsive polymeric nanoparticles for programmed site-specific drug delivery. Biomaterials 34:3647–3657

Choi Y, Kim S, Choi MH, Ryoo SR, Park J, Min DH, Kim BS (2014) Highly biocompatible carbon nanodots for simultaneous bioimaging and targeted photodynamic therapy in vitro and in vivo. Adv Funct Mater 24:5781–5789

Dai J, Lin SD, Cheng D, Zou SY, Shuai XT (2011) Interlayer-crosslinked micelle with partially hydrated core showing reduction and pH dual sensitivity for pinpointed intracellular drug release. Angew Chem Int Ed 2011:9404–9408

Dameron CT, Reese RN, Mehra RK, Kortan AR, Carroll PJ, Steigerwald ML, Brus LE, Winge DR (1989) Biosynthesis of cadmium sulphide quantum semiconductor crystallites. Nature 338:596–597

Dawidczyk CM, Russell LM, Searson PC (2014) Nanomedicines for cancer therapy: state-of-the-art and limitations to pre-clinical studies that hinder future developments. Front Chem 2:69

De B, Karak N (2013) A green and facile approach for the synthesis of water soluble fluorescent carbon dots from banana juice. RSC Adv 3:8286–8290

De Oliveira R, Zhao P, Li N, de Santa Maria LC, Vergnaud J, Ruiz J, Astruc D, Barratt G (2013) Synthesis and in vitro studies of gold nanoparticles loaded with docetaxel. Int J Pharm 454:703–711

Deng J, Lu Q, Mi N, Li H, Liu M, Xu M, Tan L, Xie Q, Zhang Y, Yao S (2014) Electrochemical synthesis of carbon nanodots directly from alcohols. Chem Eur J 20:4993–4999

Ding Y, Zhou YY, Chen H, Geng DD, Wu DY, Hong J, Shen WB, Hang J, Zhang C (2013) The performance of thiol-terminated PEG-paclitaxel conjugated gold nanoparticles. Biomaterials 34:10217–10227

Dong H, Du SR, Zheng XY, Lyu GM, Sun LD, Li LD, Zhang PZ, Zhang C, Yan CH (2015) Lanthanide nanoparticles: from design toward bioimaging and therapy. Chem Rev 115:10725–10815

Dreaden EC, Mwakwari SC, Sodji QH, Oyelere AK, El-Sayed MA (2009) Tamoxifen-poly (ethylene glycol)-thiol gold nanoparticle conjugates: enhanced potency and selective delivery for breast cancer treatment. Bioconjugate Chem 20:2247–2253

Duan Q, Cao Y, Li Y, Hu X, Xiao T, Lin C, Pan Y, Wang L (2013) pH-Responsive supramolecular vesicles based on water-soluble pillar[6]arene and ferrocene derivative for drug delivery. J Am Chem Soc 135:10542–10549

Feazell RP, Nakayama-Ratchford N, Dai H, Lippard SJ (2007) Soluble single-walled carbon nanotubes as longboat delivery systems for platinum(IV) anticancer drug design. J Am Chem Soc 129:8438–8439

Gabizon A, Shmeeda H, Barenholz Y (2003) Pharmacokinetics of pegy-lated liposomal Doxorubicin: review of animal and human studies. Clin Pharmacokinet 42:419–436

Gai SL, Li CX, Yang PP, Lin J (2014) Recent progress in rare earth micro/nanocrystals: soft chemical synthesis, luminescent properties, and biomedical applications. Chem Rev 114:2343–2389

Ge ZS, Liu SY (2013) Functional block copolymer assemblies responsive to tumor and intracellular microenvironments for site-specific drug delivery and enhanced imaging performance. Chem Soc Rev 42:7289–7325

Guo F, Kim F, Han TH, Shenoy VB, Huang J, Hurt RH (2011) Hydration-responsive folding and unfolding in graphene oxide liquid crystal phases. ACS Nano 5:8019–8025

Guo DS, Wang K, Wang YX, Liu Y (2012) Cholinesterase-responsive supramolecular vesicle. J Am Chem Soc 134:10244–10250

Haase M, Schaefer H (2011) Upconverting nanoparticles. Angew Chem Int Ed 50:5808–5829

Hong G, Robinson JT, Zhang Y, Diao S, Antaris AL, Wang Q, Dai H (2012) In vivo fluorescence imaging with Ag_2S quantum dots in the second near-infrared region. Angew Chem Int Ed 51:9818–9821

Hong G, Diao S, Antaris AL, Dai H (2015) Carbon nanomaterials for biological imaging and nanomedicinal therapy. Chem Rev 115:10816–10906

Hood MA, Mari M, Muñoz-Espí R (2014) Synthetic strategies in the preparation of polymer/inorganic hybrid nanoparticles. Materials 7:4057–4087

Hosta L, Pla-Roca M, Arbiol J, Lopez-Iglesias C, Samitier J, Cruz LJ, Kogan MJ, Albericio F (2009) Conjugation of kahalalide F with gold nanoparticles to enhance in vitro antitumoral activity. Bioconjugate Chem 20:138–146

Hsu CY, Chen CW, Yu HP, Lin YF, Lai PS (2013) Bioluminescence resonance energy transfer using luciferase-immobilized quantum dots for self-illuminated photodynamic therapy. Biomaterials 34:1204–1212

Hu SL, Niu KY, Sun J, Yang J, Zhao NQ, Du XW (2009) One-step synthesis of fluorescent carbon nanoparticles by laser irradiation. J Mater Chem 19:484–488

Idris NM, Gnanasammandhan MK, Zhang J, Ho PC, Mahendran R, Zhang Y (2012) In vivo photodynamic therapy using upconversion nanoparticles as remote-controlled nanotransducers. Nat Med 18:1580–1585

Iijima S (1991) Helical microtubules of graphitic carbon. Nature 354:56–58

Jagannadham K, Howe J, Allard LF (2010) Laser physical vapor deposition of nanocrystalline dots using nanopore filters. Appl Phys A Mater Sci Process 98:285–292

Jia X, Li J, Wang E (2012) One-pot green synthesis of optically pH-sensitive carbon dots with upconversion luminescence. Nanoscale 4:5572–5575

Jiang J, He Y, Li S, Cui H (2012) Amino acids as the source for producing carbon nanodots: microwave assisted one-step synthesis, intrinsic photoluminescence property and intense chemiluminescence enhancement. Chem Commun 48:9634–9636

Kalantar-zadeh K, Ou JZ, Daeneke T, Strano MS, Pumera M, Gras SL (2015) Two-dimensional transition metal dichalcogenides in biosystems. Adv Funct Mater 25:5086–5099

Kang SH, Bozhilov KN, Myung NV, Mulchandani A, Chen W (2008) Microbial synthesis of CdS nanocrystals in genetically engineered *E-coli*. Angew Chem Int Ed 47:5186–5189

Karimi M, Solati N, Amiri M, Mirshekari H, Mohamed E, Taheri M, Hashemkhani M, Saeidi A, Estiar MA, Kiani P, Ghasemi A, Basri SM, Aref AR, Hamblin MR (2015) Carbon nanotubes part I: preparation of a novel and versatile drug-delivery vehicle. Expert Opin Drug Deliv 12:1071–1087

Kim F, Cote LJ, Huang J (2010) Graphene oxide: surface activity and two-dimensional assembly. Adv Mater 22:1954–1958

Kim H, Lee D, Kim J, Kim T, Kim WJ (2013) Photothermally triggered cytosolic drug delivery via endosome disruption using a functionalized reduced graphene oxide. ACS Nano 7: 6735–6746

Krysmann MJ, Kelarakis A, Giannelis EP (2012) Photoluminescent carbogenic nanoparticles directly derived from crude biomass. Green Chem 14:3141–3145

Kumar A, Zhang X, Liang XJ (2013) Gold nanoparticles: emerging paradigm for targeted drug delivery system. Biotechnol Adv 31:593–606

Kumar A, Huo S, Zhang X, Liu J, Tan A, Li S, Jin S, Xue X, Zhao Y, Ji T, Han L, Liu H, Zhang X, Zhang J, Zou G, Wang T, Tang S, Liang XJ (2014) Neurpilin-1-targeted gold nanoparticles enhance therapeutic efficacy of platinum (IV) drug for prostate cancer treatment. ACS Nano 8:4205–4220

Lay CL, Liu HQ, Tan HR, Liu Y (2010) Delivery of paclitaxel by physically loading onto poly (ethylene glycol) (PEG)-graft-carbon nanotubes for potent cancer therapeutics. Nanotechnology 21:065101

Lehn JM (1988) Supramolecular chemistry—scope and perspectives: molecules, supermolecules, and molecular devices (Nobel Lecture). Angew Chem Int Ed 27:89–112

Li JM, Wang YY, Zhao MX, Tan CP, Li YQ, Le XY, Ji LN, Mao ZW (2012a) Multifunctional QD-based co-delivery of siRNA and doxorubicin to HeLa cells for reversal of multidrug resistance and real-time tracking. Biomaterials 33:2780–2790

Li ZX, Barnes JC, Bosoy A, Stoddart JF, Zink JI (2012b) Mesoporous silica nanoparticles in biomedical applications. Chem Soc Rev 41:2590–2605

Li W, Zhang Z, Kong B, Feng S, Wang J, Wang L, Yang J, Zhang F, Wu P, Zhao D (2013) Simple and green synthesis of nitrogen-doped photoluminescent carbonaceous nanospheres for bioimaging. Angew Chem Int Ed 52:8151–8155

Liu Z, Robinson JT, Sun X, Dai HJ (2008) PEGylated nanographene oxide for delivery of water-insoluble cancer drugs. J Am Chem Soc 130:10876–10877

Liu C, Zhang P, Zhai X, Tian F, Li W, Yang J, Liu Y, Wang H, Wang W, Liu W (2012a) Nano-carrier for gene delivery and bioimaging based on carbon dots with PEI-passivation enhanced fluorescence. Biomaterials 33:3604–3613

Liu S, Tian J, Wang L, Zhang Y, Qin X, Luo Y, Asiri AM, Al-Youbi AO, Sun X (2012b) Hydrothermal treatment of grass: a low-cost, green route to nitrogen-doped, carbon-rich, photoluminescent polymer nanodots as an effective fluorescent sensing platform for label-free detection of Cu(II) ions. Adv Mater 24:2037–2041

Liu K, Liu Y, Yao Y, Yuan H, Wang S, Wang Z, Zhang X (2013) Supramolecular photosensitizers with enhanced antibacterial efficiency. Angew Chem Int Ed 125:8443–8447

Liu T, Wang C, Gu X, Gong H, Cheng L, Shi X, Feng L, Sun B, Liu Z (2014) Drug delivery with PEGylated MoS_2 nano-sheets for combined photothermal and chemotherapy of cancer. Adv Mater 26:3433–3440

Lowis S, Lewis I, Elsworth A, Weston C, Doz F, Vassal G (2006) A phase I study of intravenous liposomal daunorubicin (DaunoXome) in paediatric patients with relapsed or resistant solid tumours. Br J Cancer 95:571–580

Lu Q, Yu Y, Ma Q, Chen B, Zhang H (2016) 2D transition-metal-dichalcogenide-nanosheet-based composites for photocatalytic and electrocatalytic hydrogen evolution reactions. Adv Mater 28:1917–1933

Luo Z, Ding XW, Hu Y, Wu SJ, Xiang Y, Zeng YF, Zhang BL, Yan H, Zhang HC, Zhu LL, Liu JJ, Li JH, Cai KY, Zhao YL (2013) Engineering a hollow nanocontainer platform with multifunctional molecular machines for tumor-targeted therapy in vitro and in vivo. ACS Nano 11:10271–10284

Ma X, Zhao YL (2015) Biomedical applications of supramolecular systems based on host-guest interactions. Chem Rev 115:7794–7839

Ma X, Nguyen KT, Borah P, Ang CY, Zhao YL (2012) Functional silica nanoparticles for redox-triggered drug/ssdna co-delivery. Adv Healthcare Mater 1:690–697

Ma PA, Xiao H, Li X, Li C, Dai Y, Cheng Z, Jing X, Lin J (2013) Rational design of multifunctional upconversion nanocrystals/polymer nanocomposites for cisplatin (IV) delivery and biomedical imaging. Adv Mater 25:4898–4905

Manju S, Sreenivasan K (2012) Gold nanoparticles generated and stabilized by water soluble curcumin-polymer conjugate: blood compatibility evaluation and targeted drug delivery onto cancer cells. J Colloid Interface Sci 368:144–151

Michalet X, Pinaud FF, Bentolila LA, Tsay JM, Doose S, Li JJ, Sundaresan G, Wu AM, Gambhir SS, Weiss S (2005) Quantum dots for live cells, in vivo imaging, and diagnostics. Science 307:538–544

Min Y, Mao C, Xu D, Wang J, Liu Y (2010) Gold nanorods for platinum based prodrug delivery. Chem Commun 46:8424–8426

Muhammad F, Guo M, Guo Y, Qi W, Qu F, Sun F, Zhao H, Zhu G (2011) Acid degradable ZnO quantum dots as a platform for targeted delivery of an anticancer drug. J Mater Chem 21:13406–13412

Murray CB, Norris DJ, Bawendi MG (1993) Synthesis and characterization of nearly monodisperse CdE(E = S, Se, Te) semiconductor nanocrystallites. J Am Chem Soc 115:8706–8715

Nam J, La WG, Hwang S, Yeong SH, Park N, Won N, Jung S, Bhang SH, Ma YJ, Cho YM, Jin M, Han J, Shin JY, Wang EK, Kim SG, Cho SH, Yoo J, Kim BS, Kim S (2014) pH-responsive assembly of gold nanoparticles and 'spatiotemporally concerted' drug release for synergistic cancer therapy. ACS Nano 7:3388–3402

Norman RS, Stone JW, Gole A (2013) Targeted photothermal lysis of the pathogenic bacteria, Pseudomonas aeruginosa, with gold nanorods. Nano Lett 8:302–306

Novoselov KS, Geim AK, Morozov SV, Jiang D, Zhang Y, Dubonos SV, Grigorieva IV, Firsov AA (2004) Electric field in atomically thin carbon films. Science 306:666–669

Novoselov KS, Geim AK, Morozov SV, Jiang D, Katsnelson MI, Grigorieva IV, Dubonos SV, Firsov AA (2005) Two-dimensional gas of massless Dirac fermions in grapheme. Nature 438:197–200

Park C, Youn H, Kim H, Noh T, Kook YH, Oh ET, Park HJ, Kim C (2009a) Cyclodextrin-covered gold nanoparticles for targeted delivery of an anti-cancer drug. J Mater Chem 19:2310–2315

Park S, An J, Jung I, Piner RD, An SJ, Li X, Velamakanni A, Ruoff RS (2009b) Colloidal suspensions of highly reduced graphene oxide in a wide variety of organicsolvents. Nano Lett 9:1593–1597

Patra CR, Bhattacharya R, Mukhopadhyay D, Mukherjee P (2010) Fabrication of gold nanoparticles for targeted therapy in pancreatic cancer. Adv Drug Deliv Rev 62:346–361

Peng H, Travas-Sejdic J (2009) Simple aqueous solution route to luminescent carbogenic dots from carbohydrates. Chem Mater 21:5563–5565

Qiao ZY, Zhang R, Du FS, Liang DH, Li ZC (2011) Multi-responsive nanogels containing motifs of ortho ester, oligo(ethylene glycol) and disulfide linkage as carriers of hydrophobic anti-cancer drugs. J Control Release 152:57–66

Reilly RM (2007) Carbon nanotubes: potential benefits and risks of nanotechnology in nuclear medicine. J Nucl Med 48:1039–1042

Semonin OE, Luther JM, Choi S, Chen HY, Gao JB, Nozik AJ, Beard MC (2011) Peak external photocurrent quantum efficiency exceeding 100% via meg in a quantum dot solar cell. Science 334:1530–1533

Shen HB, Bai XW, Wang A, Wang HZ, Qian L, Yang YX, Titov A, Hyvonen J, Zheng Y, Li LS (2014) High-efficient deep-blue light-emitting diodes by using high quality $Zn_xCd_{1-x}S$/ZnS core/shell quantum dots. Adv Funct Mater 24:2367–2373

Shi Q, Li Y, Xu Y, Wang Y, Yin X, He X, Zhang Y (2014) High-yield and high-solubility nitrogen-doped carbon dots: formation, fluorescence mechanism and imaging application. RSC Adv 4:1563–1566

Silverman JA, Deitcher SR (2013) Marqibo(R) (vincristine sulfate liposome injection) improves the pharmacokinetics and pharmacodynamics of vincristine. Cancer Chemother Pharmacol 71:555–564

Song XJ, Chen Q, Liu Z (2014a) Recent advances in the development of organic photothermal nano-agents. Nano Res 8:340–354

Song Y, Zhu S, Yang B (2014b) Bioimaging based on fluorescent carbon dots. RSC Adv 4:27184–27200

Sprinkle M, Ruan M, Hu Y, Hankinson J, Rubio-Roy M, Zhang B, Wu X, Berger C, de Heer WA (2010) Scalable templated growth of graphene nanoribbons on SiC. Nat Nanotechnol 5: 727–731

Sreejith S, Huong TTM, Borah P, Zhao YL (2015) Organic-inorganic nanohybrids for fluorescence, photoacoustic and Raman bioimaging. Sci Bull 60:665–678

Sun X, Liu Z, Welsher K, Robinson JT, Goodwin A, Zaric S, Dai HJ (2008) Nano-graphene oxide for cellular imaging and drug delivery. Nano Res 1:203–212

Sun D, Ban R, Zhang P, Wu G, Zhang J, Zhu J (2013) Hair fiber as a precursor for synthesizing of sulfur- and nitrogen-co-doped carbon dots with tunable luminescence properties. Carbon 64:424–434

Sun H, She P, Lu G, Xu K, Zhang W, Liu Z (2014) Recent advances in the development of functionalized carbon nanotubes: a versatile vector for drug delivery. J Mater Sci 49: 6845–6854

Sun Z, Xie H, Tang S, Yu XF, Guo Z, Shao J, Zhang H, Huang H, Wang H, Chu PK (2015) Ultrasmall black phosphorus quantum dots: synthesis and use as photothermal agents. Angew Chem Int Ed 54:11526–11530

Tang FQ, Li LL, Chen D (2012) Mesoporous silica nanoparticles: synthesis, biocompatibility and drug delivery. Adv Mater 24:1504–1534

Tang J, Kong B, Wu H, Xu M, Wang Y, Wang Y, Zhao D, Zheng G (2013) Carbon nanodots featuring efficient FRET for real-time monitoring of drug delivery and two-photon imaging. Adv Mater 25:6569–6574

Tao H, Yang K, Ma Z, Wan J, Zhang Y, Kang Z, Liu Z (2012) In vivo NIR fluorescence imaging, biodistribution, and toxicology of photoluminescent carbon dots produced from carbon nanotubes and graphite. Small 8:281−290

Tian Q, Tang M, Sun Y, Zou R, Chen Z, Zhu M, Yang S, Wang J, Wang J, Hu J (2011) Hydrophilic flower-like CuS superstructures as an efficient 980 nm laser-driven photothermal agent for ablation of cancer cells. Adv Mater 23:3542–3547

Tong L, Zhao Y, Huff TB (2007) Gold nanorods mediate tumor cell death by compromising membrane integrity. Adv Mater 19:3136–3141

Tran V, Soklaski R, Liang Y, Yang L (2014) Layer-controlled band gap and anisotropic excitons in few-layer black phosphorus. Phys Rev B 89:235319

Tu C, Zhu L, Li P, Chen Y, Su Y, Yan D, Zhu X, Zhou GG (2011) Supramolecular polymeric micelles by the host-guest interaction of star-like calix[4]arene and chlorin e6 for photodynamic therapy. Chem Commun 47:6063–6065

Vllasaliu D, Fowler R, Stolnik S (2014) PEGylated nanomedicines: recent progress and remaining concerns. Expert Opin Drug Deliv 11:139–154

Wang C, Tao HQ, Cheng L, Liu Z (2011) Near-infrared light induced in vivo photodynamic therapy of cancer based on upconversion nanoparticles. Biomaterials 32:6145–6154

Wang WW, Cheng D, Gong FM, Miao XM, Shuai XT (2012) Design of multifunctional micelle for tumor-targeted intracellular drug release and fluorescent imaging. Adv Mater 24:115–120

Wang C, Xu H, Liang C, Liu YM, Li ZW, Yang GB, Cheng L, Li YG, Liu Z (2013a) Iron oxide@ polypyrrole nanoparticles as a multifunctional drug carrier for remotely controlled cancer therapy with synergistic antitumor effect. ACS Nano 7:6782–6795

Wang J, Sahu S, Sonkar SK, Tackett KN II, Sun KW, Liu Y, Maimaiti H, Anilkumar P, Sun Y (2013b) Versatility with carbon dots—from overcooked BBQ to brightly fluorescent agents and photocatalysts. RSC Adv 3:15604–15607

Wang H, Yang X, Shao W, Chen S, Xie J, Zhang X, Wang J, Xie Y (2015) Ultrathin black phosphorus nanosheets for efficient singlet oxygen generation. J Am Chem Soc 137: 11376–11382

Wee SS, Ng YH, Ng SM (2013) Synthesis of fluorescent carbon dots via simple acid hydrolysis of bovine serum albumin and its potential as sensitive sensing probe for lead (II) ions. Talanta 116:71–76

Wu S, Butt HJ (2016) Near-infrared-sensitive materials based on upconverting nanoparticles. Adv Mater 28:1208–1226

Wu J, WangY Yang X, Liu Y, Yang J, Yang R, Zhang N (2012) Graphene oxide used as a carrier for adriamycin can reverse drug resistance in breast cancer cells. Nanotechnology 23:355101

Wu Z, Zhang P, Gao M, Liu C, Wang W, Leng F, Huang C (2013) One-pot hydrothermal synthesis of highly luminescent nitrogen-doped amphoteric carbon dots for bioimaging from Bombyx mori silk - natural proteins. J Mater Chem B 1:2868–2873

Wu WT, Liu H, Dong C, Zheng WJ, Han LL, Li L, Qiao SZ, Yang J, Du XW (2015) Gain high-quality colloidal quantum dots directly from natural minerals. Langmuir 31:2251–2255

Xu X, Ray R, Gu Y, Ploehn HJ, Gearheart L, Raker K, Scrivens WA (2004) Electrophoretic analysis and purification of fluorescent single-walled carbon nanotube fragments. J Am Chem Soc 126:12736–12737

Xu LG, Cheng L, Wang C, Peng R, Liu Z (2014) Conjugated polymers for photothermal therapy of cancer. Polym Chem 5:1573–1580

Yan H, Teh C, Sreejith S, Zhu LL, Kwok A, Fang WQ, Ma X, Nguyen KT, Korzh V, Zhao YL (2012) Functional mesoporous silica nanoparticles for photothermal-controlled drug delivery in vivo. Angew Chem Int Ed 51:8373–8377

Yang D, Yang F, Hu J, Long J, Wang C, Fu D, Ni Q (2009) Hydrophilic multi-walled carbon nanotubes decorated with magnetite nanoparticles as lymphatic targeted drug delivery vehicles. Chem Commun 4447–4449

Yang J, Choi J, Bang D, Kim E, Lim EK, Park H, Suh JS, Lee K, Yoo KH, Kim EK, Huh YM, Haam S (2011) Convertible organic nanoparticles for near-infrared photothermal ablation of cancer cells. Angew Chem Int Ed 50:441–444

Yang PP, Gai SL, Lin J (2012) Functionalized mesoporous silica materials for controlled drug delivery. Chem Soc Rev 41:3679–3698

Yang X, Yang M, Pang B, Vara M, Xia Y (2015a) Gold nanomaterials at work in biomedicine. Chem Rev 115:10410–10488

Yang K, Yang G, Chen L, Cheng L, Wang L, Ge C, Liu Z (2015b) FeS nanoplates as a multifunctional nano-theranostic for magnetic resonance imaging guided photothermal therapy. Biomaterials 38:1–9

Zhai X, Zhang P, Liu C, Bai T, Li W, Dai L, Liu W (2012) Highly luminescent carbon nanodots by microwave-assisted pyrolysis. Chem Commun 48:7955–7957

Zhang H (2015) Ultrathin two-dimensional nanomaterials. ACS Nano 9:9451–9469

Zhang H, Wang LP, Xiong HM, Hu LH, Yang B, Li W (2003) Hydrothermal synthesis for high-quality CdTe nanocrystals. Adv Mater 15:1712–1715

Zhang Q, Liu F, Nguyen KT, Ma X, Wang XJ, Xing BG, Zhao YL (2012) Multifunctional mesoporous silica nanoparticles for cancer-targeted and controlled drug delivery. Adv Funct Mater 22:5144–5156

Zhang Z, Wang J, Chen C (2013) Gold nanorods based platforms for light-mediated theranostics. Theranostics 3:223–228

Zhang Z, Wang J, Nie X, Wen T, Ji Y, Wu X, Zhao Y, Chen Y (2014a) Near-infrared laser-induced targeted cancer therapy using thermoresponsive polymer encapsulated gold nanorods. J Am Chem Soc 136:7317–7326

Zhang Q, Wang XL, Li PZ, Nguyen KT, Wang XJ, Luo Z, Zhang HC, Tan NS, Zhao YL (2014b) Biocompatible, uniform, and redispersible mesoporous silica nanoparticles for cancer-targeted drug delivery in vivo. Adv Funct Mater 24:2450–2461

Zhou J, Sheng Z, Han H, Zou M, Li C (2012) Facile synthesis of fluorescent carbon dots using watermelon peel as a carbon source. Mater Lett 66:222–224

Zhu H, Wang X, Li Y, Wang Z, Yang F, Yang X (2009) Microwave synthesis of fluorescent carbon nanoparticles with electrochemiluminescence properties. Chem Commun 5118–5120

Zhu C, Zhai J, Dong S (2012) Bifunctional fluorescent carbon nanodots: green synthesis via soy milk and application as metal-free electrocatalysts for oxygen reduction. Chem Commun 48:9367–9369

Zhuge FY, Zhang CW, Zeng CC, Liu HP (2015) Studies on PEGylated gold nanoparticles loaded with 5-hydroxydecanoate for chemo-photothermal therapy of human lung adenocarcinomas in vitro. Nano Brief Reports and Reviews 10:1550101

Conclusions

In this brief, we introduced various kinds of nanomaterial-based drug delivery carriers for cancer therapy. Precisely designed nanomaterials including organic, inorganic, and organic–inorganic hybrid nanomaterials possess increased solubility, prolonged circulation time and improved biodistribution by the utilization of the EPR effect or active targeting effect in order to alter the uptake mechanism to overcome the disadvantageous toxicity, drug resistance, and low stability of conventional chemotherapeutics. Up to date, although numerous nanocarriers have been developed to treat cancer, there are still limited nanotherapeutics approved for clinical uses. Certain crucial challenges need to be tackled, including pharmacokinetics, and biodistribution (clearance rate and half-life), biocompatibility (immunogenic response and elimination route), targeting efficiency (specificity and sensitivity) and the safety profile of nanocarriers (toxicity and off-target accumulation). Addressing these issues will allow us to create suitable nanomaterial-based drug delivery carriers for clinical cancer therapeutics. Thus, we expect more breakthrough researches for translating nanomaterial-based therapeutics into clinical uses in the near future.

T. Feng and Y. Zhao, *Nanomaterial-Based Drug Delivery Carriers for Cancer Therapy*, Nanotheranostics, DOI 10.1007/978-981-10-3299-8